CERN-ACC-2019-0052

August 2019
stephane.fartoukh@cern.ch

First High-Intensity Beam Tests with Telescopic Flat Optics at the LHC

S. Fartoukh, G. Azzopardi, R. Bruce, X. Buffat, J. Coello De Portugal, J. Dilly, E. Fol, N. Fuster-Martinez, A. Garcia-Tabares, M. Hofer, N. Karastathis, E.H. Maclean, L. Malina, A. Mereghetti, D. Mirarchi, T. Persson, M. Pojer, A. Poyet, M. Schaumann, M. Solfaroli, G. Sterbini, R. Tomas, D. Valuch, A. Wegscheider, J. Wenninger

Keywords: LHC and HL-LHC optics, ATS scheme, flat optics

Summary

The paper reports on the first high-intensity beam tests obtained with flat optics in 2018 (MD2148). This new machine configuration is described in terms of hypercycle, optics transitions, and dedicated beam gymnastics. The various commissioning steps which were needed to obtain the green light for an intensity ramp up are highlighted, in particular the optics measurements and corrections, the triplet aperture measurements, and the collimation-related activities. First collision of trains took place in the second 2018 LHC MD block. The main results are given in terms of luminosity, long-range beam-beam mitigation with lattice octupoles, and corresponding crossing angle reach.

1 Introduction

An important effort for optics developments was deployed in 2017 in order to enable first validation tests of flat optics in Run 2 [1]. The first flat-optics machine development (MD) session did actually take place at the very last MD block of the 2017 Run, still with low intensity beams, showing already very promising results, but announcing as well some challenges to overcome in terms of optics correct-ability [2]. This effort was pursued in 2018 aiming at colliding a few bunch trains in this new machine configuration, in order to draw first conclusions for the potential usage of flat optics in Run 3 [3], and for the HL-LHC [4].
The breakdown structure of the special LHC hypercycle which was used in 2018 is given in Section 2, with the different beam processes (BP) involved, described in terms of optics, various gymnastics, and knob pre-setting strategy. An overview of the various MD activities is given in Section 3. Optics measurement and correction results are reported in Section 4, while Section 5 de-

scribes the validation steps which were needed for an intensity ramp-up (triplet aperture measurement, loss maps, derivation of new TCT functions, asynchronous dump test). The results obtained during the high-intensity tests (one fill with 61 nominal bunches, one non-colliding) are concentrated in Section 6, including the beam-beam related studies which took place, and the observation of some unexpected beam instabilities, their interpretation and possible mitigation measures to keep in mind for future tests.

2 Description of the hypercycle

The targeted machine configuration was a collision flat optics with $\beta^*_{x/y} = 60/15$ cm at IP1 and 15/60 cm at IP5, an H/V alternated crossing scheme in ATLAS and CMS (i.e. swapped w.r.t. the nominal LHC configuration for triplet aperture related reasons [3]), and the usage of ATS scheme [5] to actually realize the optics. A brand new LHC hypercycle was constructed accordingly, recycling whenever possible some already existing beam processes (BP), but also building new dedicated BP's and insert them at appropriate position in the sequencer. The different strength files corresponding to the optics sequence which was used can be found in [6]. A detailed description of the hypercycle is given hereafter.

2.1 Combined ramp and squeeze

The nominal 2018 injection optics was re-used, and the combined ramp and squeeze cloned from the nominal ramp. In particular, collimators and machine protection devices were run keeping their operational settings in the ramp (within one exception recorded hereafter), even for the optics commissioning shift at low intensity. Some minor modifications were nonetheless introduced, where only a subset of the available Optics and Measurement Correction (OMC) knobs [7, 8, 9] was kept, namely: the knobs related to the global β-beating correction of the injection optics (`B1_ATS_2016_injection_globcorr` and `B2_ATS_2016_injection_globcorr`), and which are nominally vanishing at the end of the ramp (EoR), and some of the knobs attached to the local correction of the inner triplet, for beta-beating (`2017_ATS_LocalCorrection`), coupling (`2017_ATS_Inj_LocalCoupling`), and octupolar imperfections (`2017_IRNL_b4`). Another modification was applied to the collimation ramp functions, namely a tightening by 219 μm of the IR6 TCDQ and TCSP functions for Beam 2 at the end of the ramp (via a linear trim applied between 6.0 and 6.5 TeV), leading to a normalised TCDQ gap of $6.9\,\sigma$ when arriving at flat-top energy. This trim was still inside the ± 400 μm dump threshold tolerance (and within the $\pm$ 14 % relative margin coming from the BETS). It was needed to "compensate" for the reduction of the Beam 2 β-function at the TCDQ during the telescopic squeeze, ensuring a normalised gap of $7.3\,\sigma$ for the Beam 2 TCDQ at the end of the squeeze (instead of $7.8\,\sigma$ otherwise).

2.2 Gymnastic at flat-top energy

Arriving at flat-top energy ($\beta^* = 1$ m at IP1 and IP5), the three following beam processes (BP) were played in sequence:

TELE-ATS_knobs-2017_V1_ATSFlat, to transpose the standard correction knob values into the so-called TELE knobs [5] (acting only on the lattice corrector of the sectors 23, 34, 67 and 78, for tune, coupling and chromaticity), and to shift the working point from (62.275/60.295)[1] to (62.28/60.31)[2]. The duration of this beam process (recycled from the 2017 flat ATS MD) is found to be 210 seconds (limited by the maximum acceleration rate of the skew quadrupole circuits).

QCHANGE-6.5TeV-ATSFlat-2018_V1, to reach the collision tune (.31/.32) using the corresponding TELE knobs. The fact that this BP was not combined with the previous one is historical. Indeed, both for the first flat-optics MD (2017), and the first 2018 tests with low intensity beams, the Q-change BP was actually played at the end of the telescopic squeeze (as it is traditionally the case for ATS MDs in order to minimise the impact of linear coupling during optics commissioning campaigns). Later on, it was however decided to insert it in the sequencer at larger β^*, as it is the case for the nominal LHC hypercycle at the end of the ramp, in order to further improve the horizontal MKD-TCT phase advances by up to $0.03 \times 360^\circ = 10.8^\circ$ (except for the MKD-TCT.R5B2 phase which is not impacted at all by the Q-change BP).

BUMPS-INVERSION-2018_V1, to reduce the crossing angle in IR1 and IR5 from 160 μm (nominal EoR value in 2018) down to 150 μrad, and then rotate the crossing and parallel separation planes in ATLAS and CMS. The objective of this BP is to pass from the nominal V/H crossing configuration in IR1/5, to a H/V crossing configuration. During this process, the crossing planes in ATLAS and CMS are always kept perpendicular to each other, in order to maximize some long-range beam-beam self-compensation between IR1 and IR5. More precisely, from the (2018) upwards vertical crossing angle in IR1, and outwards horizontal crossing in IR5, the crossing angles become horizontal outwards and vertical downwards in IR1 and IR5, respectively, under the action of this beam process (see Fig. 1). This gymnastic is mandatory to liberate enough aperture for the squeeze in flat mode, when strongly reducing β^* in the plane corresponding to the flat part of the beam-screen (see Fig. 2), while crossing in the plane of largest β^*. The duration of this beam process is 280 seconds. In principle, this BP could take place immediately after the ramp, before any other knob manipulations, in particular with maximal fractional tune split (see Section 6 for a recommendation in this direction).

2.3 Pre-squeeze

The nominal optics pre-squeeze sequence was re-used, but truncated at $\beta^* = 65$ cm (see Tab. 1). A small reduction of the crossing angle in IR1 and IR5, from 150 μrad down to 130 μrad, and of the parallel separation, from 0.55 mm down to 0.3 mm, was also included in the corresponding BP (SQUEEZE-6.5TeV-ATS-1m-65cm-2017_V1). The OMC knob pre-setting strategy followed that previously mentioned for the clone of the nominal ramp. In particular, the nominal settings of the non-linear triplet corrector magnets other than the octupolar ones (namely the $a_3/b_3/a_4$ corrector magnets) were not re-used since they were optimized for feed-down effects in the nominal cycle (where the orientation of the crossing planes in IR1 and IR5 does not correspond to the ones actually specified for flat optics). In addition, the relative variations of the standard knobs for tune, coupling, and chromaticity knobs, as measured in nominal operation from $\beta^* = 1$ m to 65 cm, were directly used to further trim the corresponding TELE knobs, prior to the first 2018 MD. This beam process was systematically played with the nominal collision tunes

[1] LHC-2018 injection tunes for 25 ns operation in the presence of e-cloud.

[2] Design report injection tunes.

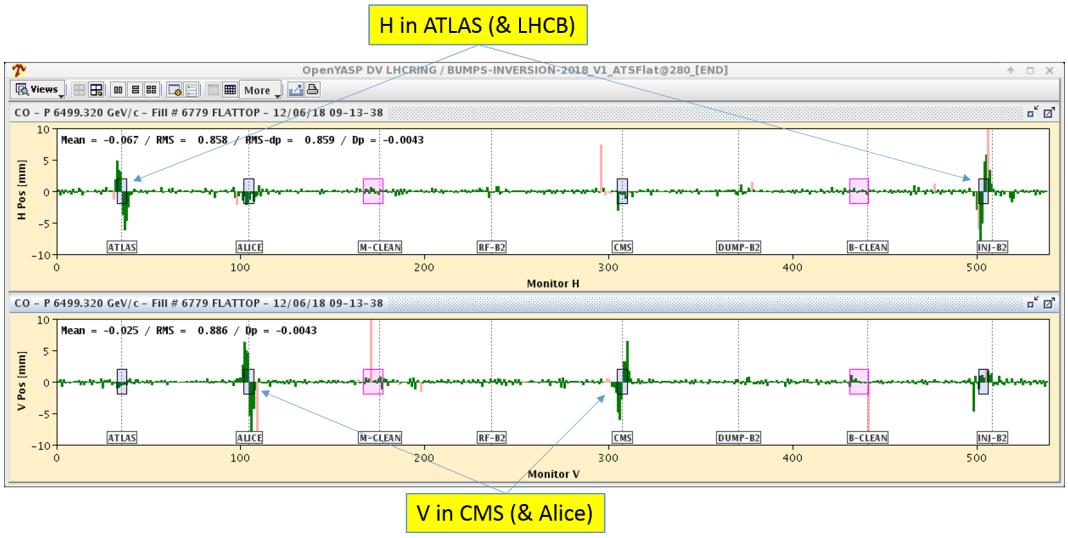

Figure 1: Typical closed orbit snapshot taken after the crossing bump rotation BP. Beam 2 is shown with negative H crossing in ATLAS and positive V crossing in CMS.

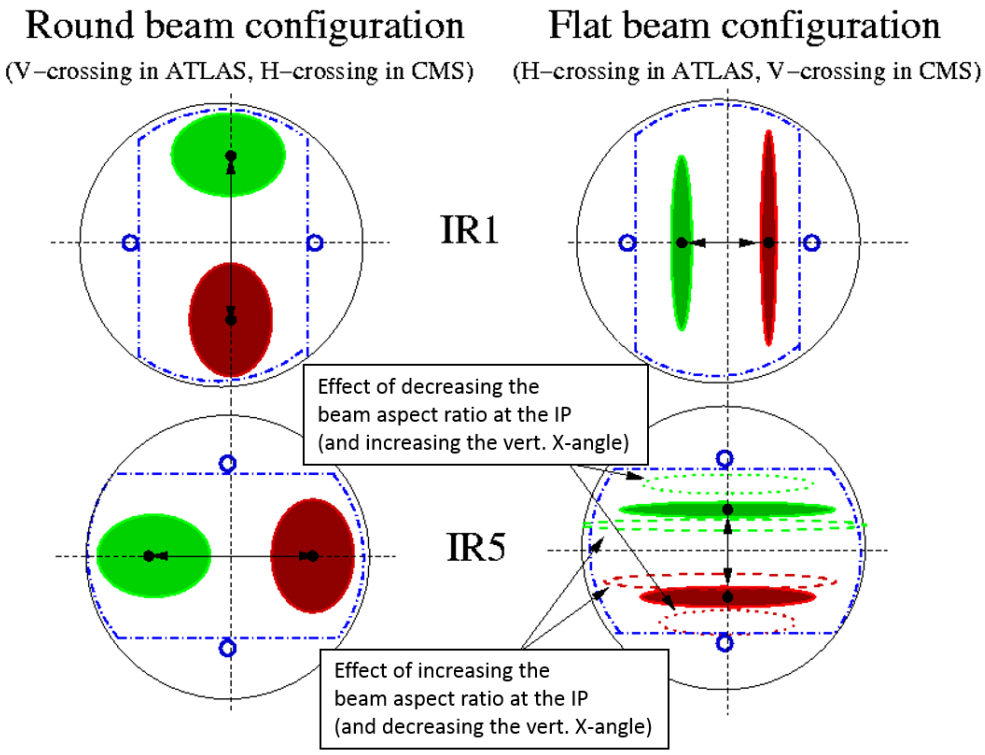

Figure 2: Sketch for the beam footprint in the inner triplets of IR1 (top) and IR5 (bottom), for round (left) and flat (right) optics configurations. The small circles on the left/right or top/bottom sides of the (out-of-scale) beam-screens represent the helium capillaries, reducing the mechanical aperture of the inner triplet by about 2×5 mm in one of the two transverse planes.

Matched Point	Time [s]	Parabolic fraction [%]	Optics name in LSA	β^* [cm] at IP1 and IP5
1	0	0	R2017a_A100C100A10mL300	100
2	53	19	R2017a_A80C80A10mL300	80
3	110	18	R2017a_A65C65A10mL300	65

Table 1: Structure and timing of the ATS pre-squeeze from $\beta^* = 1$ m down to $\beta^* = 65$ cm at IP1 and IP5 (LSA beam process `SQUEEZE-6.5TeV-ATS-1m-65cm-2017_V1`). The half crossing angle and parallel separation in IR1 and IR5 are linearly reduced from $[150\,\mu\text{rad},\ 0.55\,\text{mm}]$ down to $[130\,\mu\text{rad},\ 0.30\,\text{mm}]$. In practice, the quadrupole settings corresponding to two consecutive optics (matched points) are connected with Parabolic-Linear-Parabolic (PLP) functions, with the additional constraint of zeroing at the matched points the current slope dI/dt of each circuit involved. This "rounding in/out" procedure takes a non-negligible fraction of the overall time, reported above as "parabolic fraction".

$Q_{x/y} = 62.31/60.32$ [except for the first optics commissioning MD where the nominal injection tunes of (62.28/60.31) were kept till the end of the squeeze, see discussion on the Q-change BP in Sub-Section 2.2].

2.4 Telescopic squeeze "14-41"

Using the ATS telescopic techniques, i.e. trimming the IPQ circuits in IR8, IR2, IR4 and IR6, the telescopic squeeze BP (`SQUEEZE-6.5TeV-ATS-65cm-60_15cm-2017_V1`) further reduced β^* by a factor of 4 in the parallel separation plane at IP1 and IP5, that is in the vertical plane for ATLAS and horizontal plane for CMS, while keeping it constant in the crossing plane. For practical reasons, the first step of this BP combines a small pre-squeeze segment, from $\beta^* = 65$ cm down to $\beta^* = 60$ cm at IP1 and IP5, with a first segment for the telescopic squeeze proper (in the sense of the usage of the IPQ circuits, in IR1/5 for the pre-squeeze, and exclusively in IR8, IR2, IR4 and IR6, for the telescopic squeeze). This means that the final pre-squeezed β^* was actually 60 cm at IP1 and IP5 (a matched point which did not exist in the nominal pre-squeeze sequence), and that the actual optics at the end of this beam process was flat in IR1 and IR5, with $\beta^*_{x/y} = 60/15$ cm at IP1, and $\beta^*_{x/y} = 15/60$ cm at IP5.
This beam process was played at constant crossing scheme, in particular with $130\,\mu$rad for the half-crossing angle in IR1 (H) and IR5 (V). The OMC and `TELE` knobs were also preset to be constant over the telescopic squeeze, defined by continuity from the previous BP. In particular, the telescopic squeeze was played with the nominal collision tunes $Q_{x/y} = 62.31/60.32$ (except for the first optics commissioning MD). In addition, two OMC knobs, calculated from the 2017 flat-optics MD [2], were directly re-used, namely `2017_Local_flat_ATS` (local triplet optics correction) and `2017_Coupling_Flat_ArcByArc_B1` (arc-by-arc coupling correction for Beam 1). The timing structure of this beam process is reported in Tab. 2, showing a total duration in the range of 500 seconds (at 6.5 TeV beam energy).

Matched Point	Time [s]	Parabolic fraction [%]	Optics name in LSA	β^* [cm] H/V at IP1-5
1	0	0	R2017a_A65C65A10mL300	65.0/65.0 – 65.0/65.0
2	109	38	R2017aT65_A60_51C51_60A10mL300	60.0/51.0 – 51.0/60.0
3	210	39	R2017aT65_A60_41C41_60A10mL300	60.0/41.0 – 41.0/60.0
4	306	40	R2017aT65_A60_31C31_60A10mL300	60.0/31.0 – 31.0/60.0
5	427	36	R2017aT65_A60_21C21_60A10mL300	60.0/21.0 – 21.0/60.0
6	526	35	R2017aT65_A60_15C15_60A10mL300	60.0/15.0 – 15.0/60.0

Table 2: Structure and timing of the flat telescopic squeeze (SQUEEZE-6.5TeV-ATS-65cm-60_15cm-2017_V1) from $\beta^* = 65$ cm [telescopic indexes (1×1)-(1×1)] down to $\beta^*_{x/y} = (60/15) - (15/60)$ cm at IP1-5 [telescopic indexes (1×4)-(4×1)]. The half crossing angle and parallel separation are kept constant in IR1 and IR5, set to 130 μrad and 0.30 mm, respectively. For practical reasons, the first telescopic step was combined with a small continuation of the pre-squeeze sequence, from $\beta^* = 65$ cm down to $\beta^* = 60$ cm in round optics mode.

2.5 Collision

The parallel separation was collapsed at all 4 IPs (w/o IP shift, neither at IP2 nor at IP5) using the beam process PHYSICS-6.5TeV-ATSFlat-2018_V1. A small tune shift from (.31/.32) to (.317/.323) was also preset by default in the Physics BP, as this working point was expected to be better for dynamic aperture, in particular partially compensating for the negative long-range beam-beam induced tune shift, which is zero for round optics with alternated V/H crossing in IR1 and IR5, but not for flat optics (see [3]).

2.6 Other settings: OMC knobs, TCT, ADT, Q', octupoles

2.6.1 OMC knobs

Following the optics commissioning shift, new OMC knobs, for coupling and β-beating, were calculated and inserted in the telescopic squeeze beam process, in particular a new type of knob consisting in an orbit bump in sector 45 in order to mimic the action of a standalone quadrupole at mid-arc through feed-down effect in a few arc sextupoles (see Section 4 for more detail).

2.6.2 TCT

Following the validation shift with setup beams, new TCT functions (N-σ and center) were prepared, in particular for the crossing angle rotation beam process, the pre-squeeze with simultaneous crossing angle reduction in IR1 and IR5, and the telescopic squeeze. The TCT settings were in particular kept constant in mm during the tele-squeeze, corresponding to asymmetric normalised settings (between planes) at end of the process, namely $8\,\sigma$ in the parallel separation plane of smallest β^*, and $9\,\sigma$ in the other (crossing) plane (see Section 5 for more detail).

2.6.3 ADT

Due to non-nominal working point management, but also and mainly due the substantial changes of the IR4 optics during the telescopic squeeze, new ADT settings (BPM phases) were generated.

2.6.4 Q'

As it is traditionally the case for most ATS MDs, the beam processes were prepared with a linear chromaticity set to 10 units (using exclusively the corresponding `TELE` knobs when the ramp is finished).

2.6.5 Octupole

The octupole (MO) settings were kept nominal till the end of the pre-squeeze down to $\beta^* = 65$ cm (with positive polarity, and a knob value set to -2.5 corresponding to 470 A at flat-top energy). During the tele-squeeze, the MO current was however gradually ramped down to nearly 200 A at the end of the process, in order to profit from the increasing tele-index and subsequent boost of tune spread at constant MO current [3]:

$$\begin{cases} \dfrac{\partial Q_x}{\partial J_x} = \dfrac{\partial Q_y}{\partial J_y} \propto \dfrac{1}{8}\left[\left(r_{||}+\dfrac{1}{r_{||}}\right)^2 + \left(r_X+\dfrac{1}{r_X}\right)^2\right] \\ \dfrac{\partial Q_x}{\partial J_y} = \dfrac{\partial Q_y}{\partial J_x} \propto \dfrac{1}{2}\left[1+\dfrac{1}{4}\left(r_{||}+\dfrac{1}{r_{||}}\right)\left(r_X+\dfrac{1}{r_X}\right)\right] \end{cases}, \tag{1}$$

with $r_{||} \equiv 4$ and $r_X \equiv 1$ denoting the telescopic indexes reached at the end of the squeeze in the parallel separation plane and in the crossing plane, respectively. The telescopic squeeze therefore gave an amplification factor of 2.76 and 1.56 for the direct and cross anharmonicity terms, respectively. As understood later on, while the direct term is relevant for negative octupole polarity, the beam stability is mainly sensitive to the cross term for positive MO polarity. Retrospectively, this means that ~ 300 A, instead of ~ 200 A, for the MO current at the end of the telescopic squeeze would have been a less risky choice for the high-intensity tests (see Section 6).

3 Overview of the 2018 flat-optics MDs

All the activities were carried out during the first and second LHC MD blocks of 2018. Activities in MD1 were dedicated to setting up the machine, in order to validate this new LHC configuration for bunch trains in MD2. All timetable below are given in Geneva local time.

Two shifts were assigned in MD1:

- Tuesday 12$^{\text{th}}$ June 2018, between 07:00 and 17:00 (10 h + 2 h recovery). This shift [10, 11] was mainly devoted to the demonstration of the OP mechanics, optics measurements and correction, and aperture measurements of the inner triplet (IT). One fill (**fill 6779**) was necessary, with only a pilot bunch. While the optics commissioning was successful, a premature beam dump, caused by an electrical glitch in IR4, prevented aperture measurements to be carried out;

- Sunday 17$^{\text{th}}$ June 2018, between 12:00 and 20:00 (8 h + 2 h recovery). Two fills were used [12, 13]:

  fill 6814 this fill with probes allowed to carry out the aperture measurements at β^*=65 cm (at the end of the pre-squeeze, i.e. round optics) with the crossing planes rotated;

  fill 6815 this fill with set-up beams (i.e. two nominal bunches and some pilots) allowed (i) to find collisions in the four experimental IRs, (ii) to carry out aperture measurements at the end of the telescopic squeeze ($\beta^*_{X/\!/} = 60/15$ cm), (iii) to align the TCTs at every static point of the hyper-cycle in order to prepare detailed TCT centre functions for MD2, and (iv) to measure first loss maps (LM) at end of squeeze with aligned TCTs. Loss maps at β^*=65 cm were performed as well, with TCTs centered "on-the-fly" and set to 8 σ and 9 σ on the parallel separation and crossing planes, respectively, in order to discard any possible immediate show-stopper in this new configuration with the crossing planes rotated in IR1 and IR5.

The programme continued in MD2 with two shifts allocated:

- Monday 23$^{\text{rd}}$ July 2018, between 07:00 and 13:00 (6 h + 2 h recovery). This shift was mainly devoted to validating the machine with loss maps, in order to obtain the green light to inject unsafe beams (trains) in the second shift. Two fills with set-up beams were needed [14]:

  fill 6962 this fill was prematurely dumped by a mismatch in energy and β^* limits. Nevertheless, LMs at the end of the bump rotation beam process (i.e. $\beta^* = 1$ m, see Sec. 2.2) could be taken;

  fill 6963 this fill was dedicated to the full LM campaign, and an asynchronous dump test which successfully took place.

- Saturday 28$^{\text{th}}$ July 2018, between 22:00 and 06:00 (8 h), for long-range beam-beam studies combined with octupole tests. The MD activity had a very difficult start, since 4h were lost due to an access to fix the QPS filter of the RCD and RCS circuits of sector 78, and an XPOC reset of the LBDS of Beam 2 after the spurious trigger which took place in the previous MD [15].

4 Optics measurement and correction

The first shift of the 2018 flat-optics programme was dedicated to optics (re-)commissioning, in particular to an iteration on the measurements and corrections performed during the flat-optics MD of 2017. One important outcome from the 2017 MD was the observation of an incompressible horizontal β-beating in arc 45, which was impossible to correct below the 20 % level using traditional correction techniques [2]. After subsequent studies, it was found that the likely cause of this uncorrectable β-beating was a local error in the middle of the arc (not understood yet), further amplified by the large β-function in the region due to the large telescopic index. The absence of standalone quadrupoles in the LHC arcs motivated the idea to resort to orbit bumps in the main sextupoles, for a quasi-local correction of the β-beating via quadrupolar feed-down effects. The corresponding knob was computed before the first 2018 MD (but only trimmed in during the MD).

Knob	Trim [10^{-6}]
RQ10.R4B1	20 m^{-2}
RCBH16.R4B1	8 rad
RCBH20.R4B1	16 rad
RCBH24.R4B1	16 rad
RCBH28.R4B1	8 rad

Table 3: Local arc correction computed for Beam 1 and arc 45 before the MD, and trimmed in during the optics commissioning shift at $\beta^*_{X/||} = 60/15$ cm. It combines a trim of Q10 on the right side of IR4 (LSA knob `2018_flat_q10r4_linked_to_orbitbump`) with an orbit bump that peaks to 1.5 mm in the main sextupoles MS.18R4.B1, MS.22R4.B1 and MS.26R4.B1 (`2018_flat_orbitbump_arc45`). These three sextupole magnets belong to the focusing sextupole family of arc 45 which participates to the chromatic correction of the IR5 triplets.

The matrix coefficients of the knob are given in Table 3.
Then, from the 2017 MD, only a small correction of the IR1 triplet was left trimmed in (see Table 4), together with an arc by arc coupling correction knob for Beam 1 (see also section 2.4). The global corrections of Beam 1 were removed in view of the new correction in mind with orbit bumps. The Beam 2 correction from 2017 was also removed, because computed using the ADT in AC-dipole mode, giving de facto a sub-optimal accuracy.

Corrector	Trim [$10^{-6}m^{-2}$]
MQXB2.R1	0.4
MQXA3.L1	1.1
MQXA1.L1	1.1
MQXB2.L1	-1.1

Table 4: IR1 triplet correction (LSA knob `2017_Local_flat_ATS`), in addition to the nominal one, calculated from the 2017 flat-optics MD, and kept trimmed in for the 2018 optics recommissioning shift.

4.1 Optics measurements at $\beta^*_{X/||} = 60/15$ cm

At the end of the telescopic squeeze ($\beta^*_{X/||} = 60/15$ cm), few AC-dipole kicks were used to remeasure the optics and to compute coupling corrections. The coupling correction shown in Table 5 was applied.

Knob	Trim [10^{-3}]
Beam 2 Imag	-7.5

Table 5: Coupling correction trimmed in at $\beta^*_{X/||} = 60/15$ cm.

The optics measurement showed a β-beating compatible with the 2017 observations (see Figs. 3). As already stated, the 2017 measurement of Beam 2 was done using the ADT in AC-dipole mode, which explains the large error bars in Fig. 3(b). For reasons that remain unexplained, very high beam losses were observed during the AC-dipole excitations of Beam 1, even for low excitations.

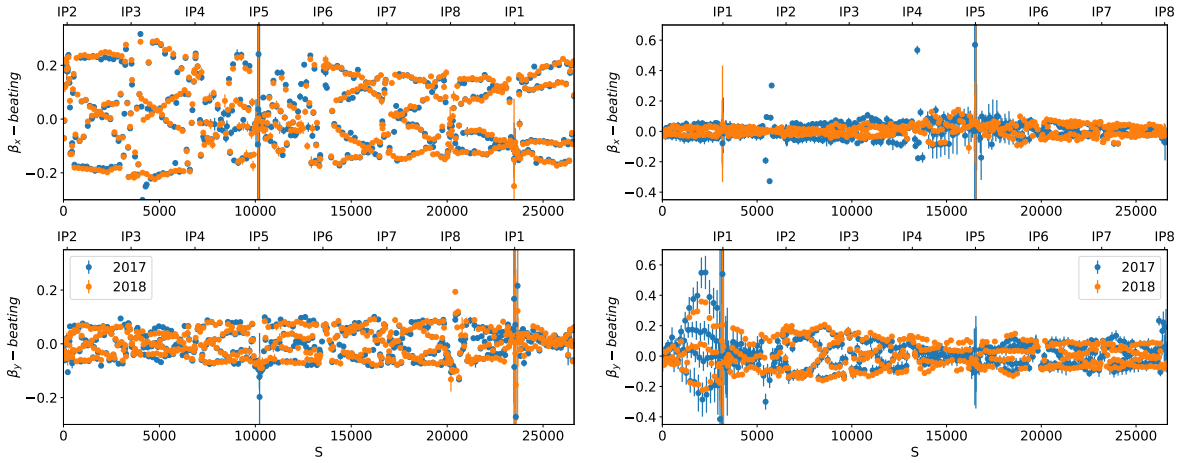

(a): Beam 1 (b): Beam 2

Figure 3: Horizontal (top) and vertical (bottom) β-beating measurement at $\beta^*_{X/||} = 60/15$ cm, for Beam 1 (left) and Beam 2 (right): comparison between 2017 and 2018 results before any new correction (except the LSA knob `2017_Local_flat_ATS` and `2017_Coupling_Flat_ArcByArc_B1`). In 2017, Beam 2 was measured using the ADT in AC-dipole mode, which explains the larger error bars on the blue markers of the right picture.

4.2 Local arc optics correction with orbit bumps

Considering the good agreement between the 2017 and 2018 optics measurements, it was decided to apply the local arc correction using the Q10.R4B1 and MCB trims shown in Table 3. Two knobs where created and trimmed in, `2018_flat_q10r4_linked_to_orbitbump` for Q10, and `2018_flat_orbitbump_arc45` for the orbit bump. The corresponding orbit from YASP is shown in Figure 4, where horizontal orbit excursions of 1.5 mm are clearly visible at MS.18R4.B1, MS.22R4.B1 and MS.26R4.B1, as expected. The trim caused as well a tune shift of about 1.3×10^{-2} in the horizontal plane, which was automatically compensated by the tune feedback system.

The optics was remeasured after trimming the two knobs of above. The result is reported in Figure 5 (Beam 1), showing a local improvement of the horizontal β-beating by about 20 % in arc 45, and a global improvement by about 10 % all around the machine. For a sake of completeness, Figure 6 compares the expected result, as simulated, to the actual one, as measured. Retrospectively, the correction efficiency is found to be slightly better than expected in the second half of arc 45, but at the cost of some degradation in the rest of the machine.

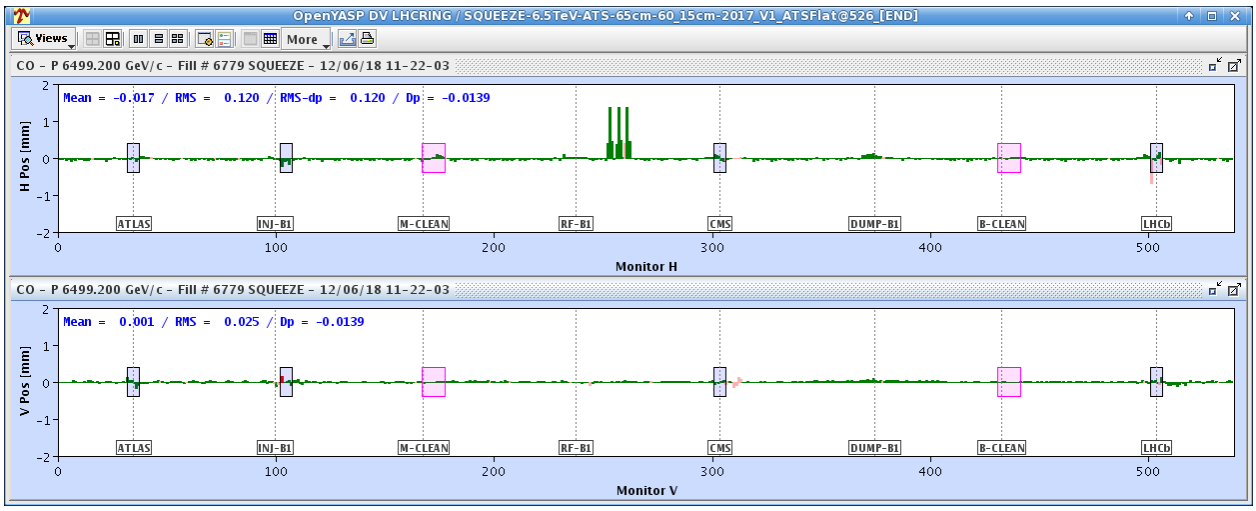

Figure 4: Capture of the YASP application showing the measured orbit after applying the horizontal orbit bump in arc 45. The reference orbit was flat, with the crossing bumps switched off in the four experimental insertions.

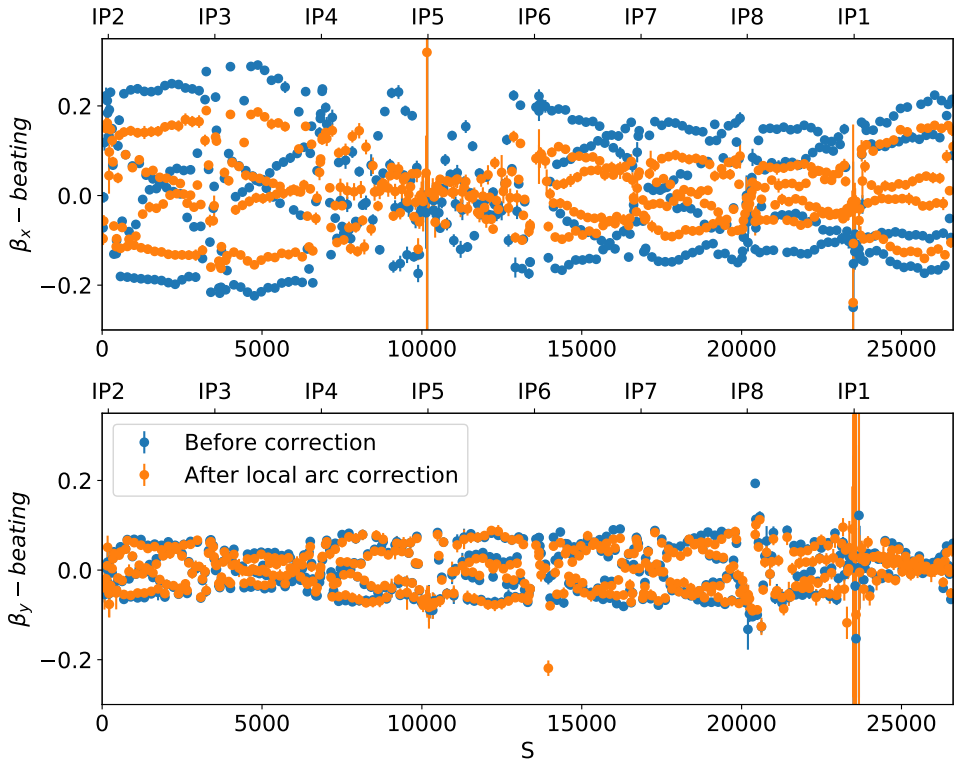

Figure 5: Beam 1 horizontal (top) and vertical (bottom) β-beating measurement results at $\beta^*_{X/||} = 60/15$ cm, before and after applying the local correction in arc 45. The correction led to a local improvement of the horizontal β-beating by about 20 % in arc 45, and a global improvement by about 10 % in the rest of the ring. The correction was transparent for the vertical plane.

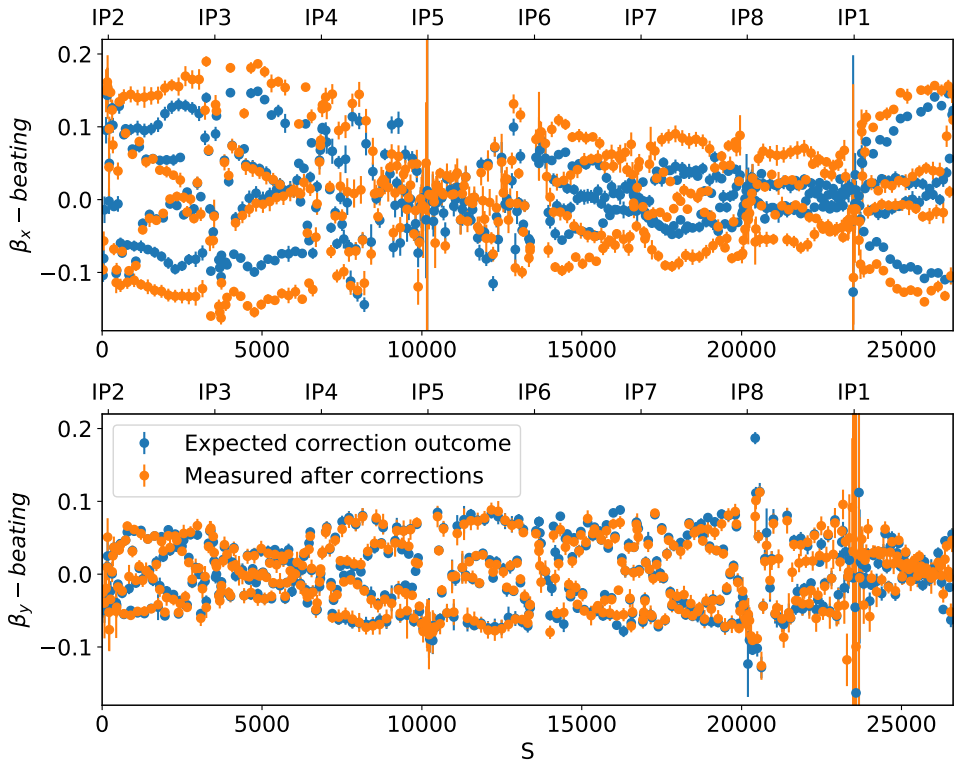

Figure 6: Comparison between measurement and prediction for the β-beating after the local correction in arc 45. The second half of the arc 45 is found to be slightly better corrected than expected, but at the cost of increasing the overall β-beating all around the machine.

4.3 Global optics corrections at $\beta^*_{X/||} = 60/15$ cm

Since the β-beating was peaking at 40 % for Beam 2 [with no correction yet, see Fig. 3(b)], and still at about 20 % for Beam 1 (see Fig. 5), it was decided to compute global corrections. To this aim, both the dispersion and β^* (from K-modulation) needed to be measured, in addition to the standard on-momentum $\beta-$beating measurement.

Due to the high beam losses observed for Beam 1 during AC-dipole excitation, and rather than using additional off-momentum AC-dipole kicks to measure the normalized dispersion, the 3-dimensional excitation technique [16] was applied. The corresponding dispersion measurement results are shown in Figure 7 (deviations with respect to the model for both beams). The coupling was then measured and corrected, in preparation for the K-modulation measurements. The correction shown in Table 6 was trimmed in.

Knob	Trim [10^{-3}]
Beam 1 Real	3.4
Beam 2 Real	2.0
Beam 2 Imag	2.0

Table 6: Coupling correction trimmed in at $\beta^*_{X/||} = 60/15$ cm, before the K-modulation measurements.

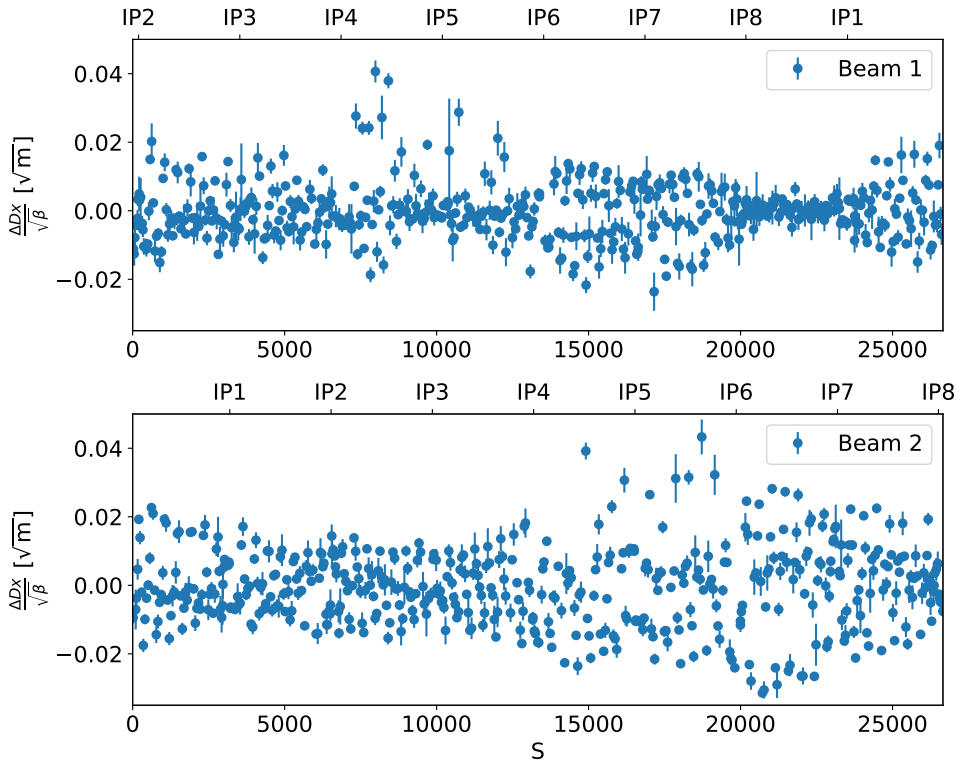

Figure 7: Beam 1 (top) and Beam 2 (bottom) horizontal normalized dispersion (deviations with respect to the model) before global correction, measured using 3-dimensional beam excitations.

K-modulation was applied to measure β^* in both planes at IP1 and IP5. The results are reported in Table 7, together with the phase advance deviations with respect to the model, computed both with K-modulation and the AC-dipole kicks, aiming at a self-consistency check of the results. The quality of the tune measurement during the K-modulation in IR1 was quite poor for Beam 1, featuring significantly higher noise than in the vertical plane, and artifacts across the signal (see Fig. 8). This is the reason of the very large error reported in Table 7 for the horizontal β^* measured for Beam 1 at IP1, which therefore should be discarded. Within this exception, all the other results were found reliable enough to be used for the global correction, with in particular a maximum β^* mismatch of 28 % obtained for Beam 1 at IP5 in the horizontal plane.

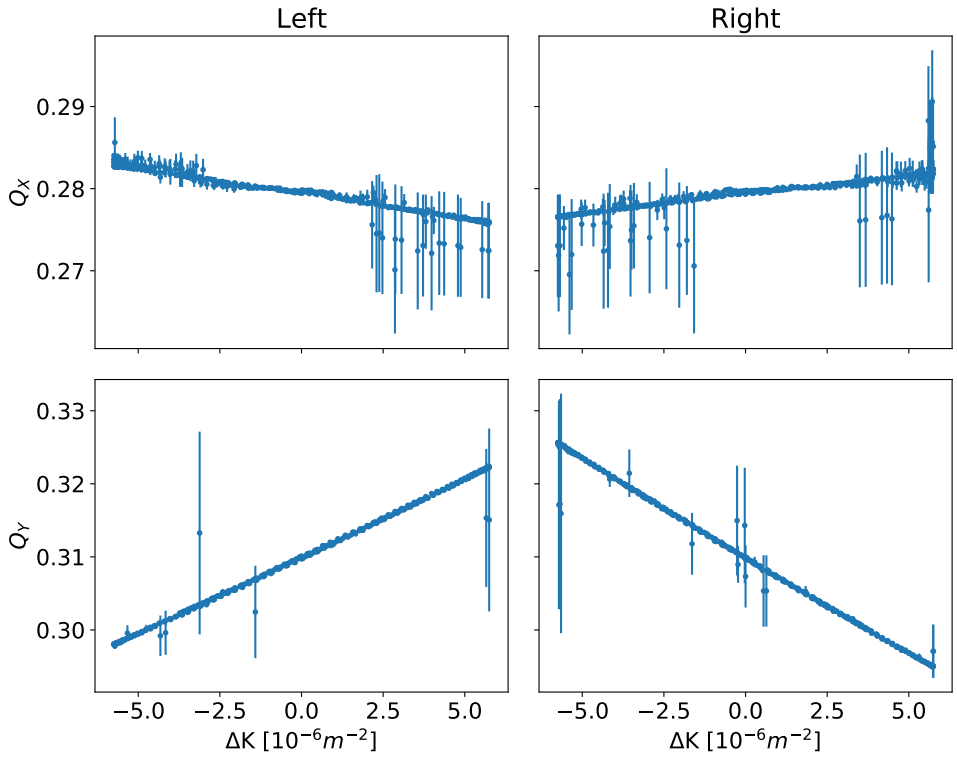

Figure 8: K-modulated tunes measured for Beam 1 before global correction, as a function of the current variations in Q1.L1 and Q1.R1. The tune signal in the horizontal plane was significantly more noisy than in the vertical plane, showing also artifacts across the measurement. This is the likely cause of the poor β^* measurement obtained for Beam 1 at IP1 in the horizontal plane (see Tab. 7).

			β^* [m]	waist [m]	$\Delta\phi_{K-mod}$ $[2\pi 10^{-4}]$	$\Delta\phi_{kicks}$ $[2\pi 10^{-4}]$
Beam 1	IP1	Hor.	0.83 ± 0.03	0.32 ± 0.03	**-26** ± 4	-6 ± 7
		Vert.	0.179 ± 0.007	-0.064 ± 0.008	-2.7 ± 1.0	1 ± 3
	IP5	Hor.	**0.192** ± 0.009	-0.082 ± 0.008	-4.5 ± 1.3	6 ± 3
		Vert.	0.675 ± 0.003	0.084 ± 0.012	-4.8 ± 0.5	10 ± 9
Beam 2	IP1	Hor.	0.575 ± 0.001	0.000 ± 0.014	8.66 ± 0.10	4 ± 3
		Vert.	0.162 ± 0.002	0.024 ± 0.006	-0.3 ± 0.3	-0.8 ± 2.0
	IP5	Hor.	0.146 ± 0.002	-0.017 ± 0.005	1.9 ± 0.2	1 ± 3
		Vert.	0.639 ± 0.001	0.024 ± 0.011	-0.04 ± 0.16	-

Table 7: K-modulation measurement results at $\beta^*_{X/||} = 60/15$ cm, after the local arc correction for Beam 1, but before any correction for Beam 2. The phase advance deviations w.r.t. the model, as computed from K-modulation and AC-dipole kicks, are also shown. Accordingly, the β^*_x measurement at IP1 shall be discarded for Beam 1. All the other measurements seem to be reliable enough, with a maximum β^* mismatch of 28 % which is found for Beam 1 at IP5 in the horizontal plane.

Global corrections were then computed for both beams using the K-modulation results as additional constraints. Two knobs were generated: `2018_global_ats_flat_b1` for Beam 1 and `2018_global_ats_flat_b2` for Beam 2. The β-beating measurement after global corrections can be seen in Figure 9 for Beam 1 and Figure 10 for Beam 2. For Beam 1, the peak β-beating reaches the 15 % level in arc 45 again, indicating that the global correction is partially opposing the local correction with orbit bumps. This interplay should be further studied to understand how to better combine these two correction techniques. The correction was kept anyway as the β-beating around the machine was greatly reduced. For Beam 2 the global correction was very successful, except in arc 81 in the vertical plane, where the β-beating could only be reduced to the 20 % level. This region, where the vertical telescopic index is set to 4, shows symptoms which are similar to Beam 1 in arc 45. As for Beam 1, a local correction of Beam 2 with orbit bumps in arc 81 would have certainly helped.

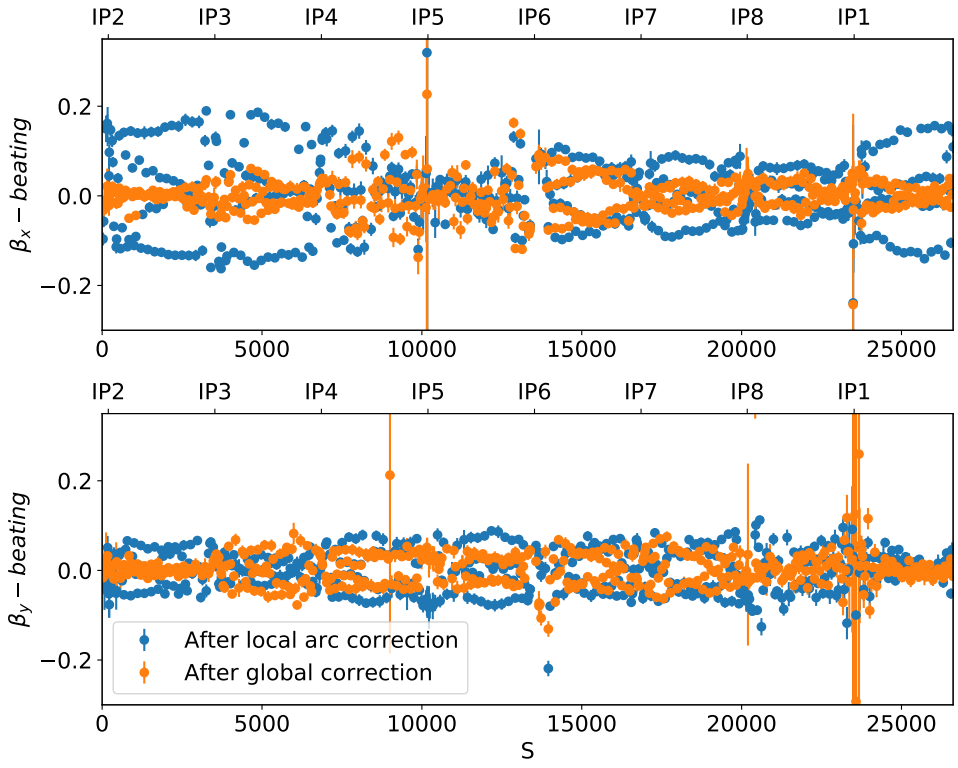

Figure 9: β-beating measurement results for Beam 1, after local arc correction and after global correction. The β-beating was reduced to about 10 % globally, except in arc 45 where it rose again up to 15 %.

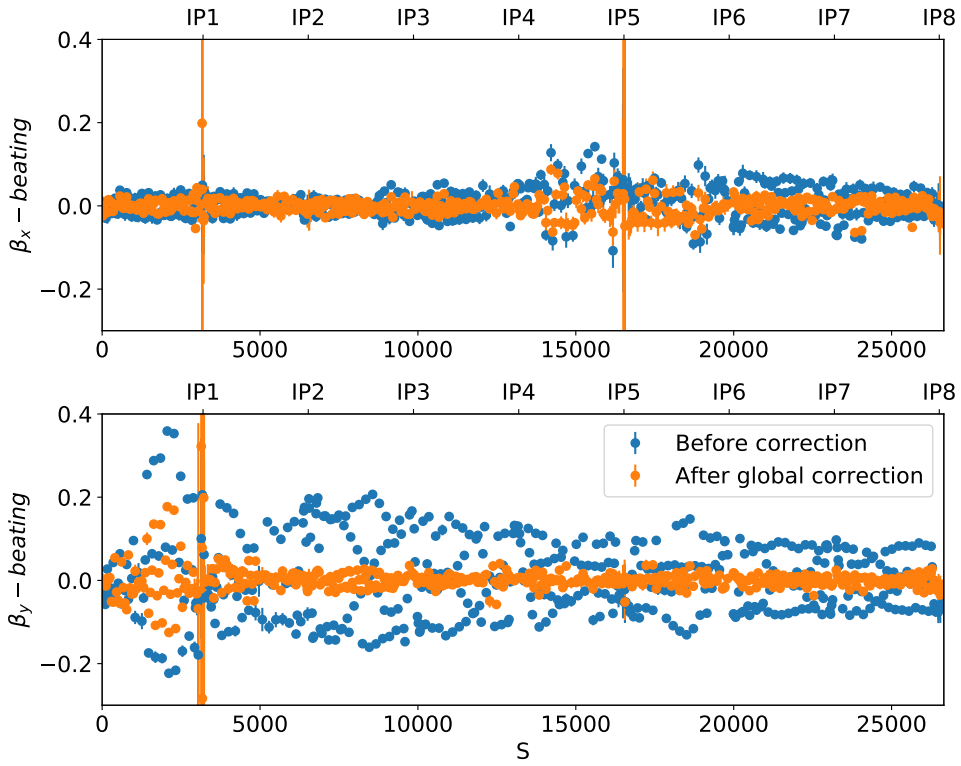

Figure 10: β-beating measurement results for Beam 2, before and after global correction. The residual β-beating reached the 5 % level after correction, except in arc 81 in the vertical plane, where the global correction was unable to bring the peak β-beating below 20 %.

The coupling correction shown in Table 8 was then applied before new K-modulation measurements in order to assess the final β^* values after global correction.

Knob	Trim [10^{-3}]
Beam 1 Real	4.0
Beam 1 Imag	-2.6
Beam 2 Imag	2.2

Table 8: Coupling correction trimmed in at $\beta^*_{X/||} = 60/15$ cm after global correction.

The results of the K-modulation measurements after global correction are shown in Table 9. Once again, the tune measurement in the horizontal plane was poor during the K-modulation in IR1, making the β^*_x measurement unusable for Beam 1 at IP1. All the other results show an improvement of the β^* mismatch thanks to the global correction. The largest mismatch is still observed for Beam 1 at IP5 in the horizontal plane, at the level of 20 %.

			β^* [m]	waist [m]	$\Delta\phi_{K-mod}$ $[2\pi 10^{-4}]$	$\Delta\phi_{kicks}$ $[2\pi 10^{-4}]$
Beam 1	IP1	Hor.	1.0 ± 1.2	0.5 ± 0.5	**-50 ± 160**	0 ± 8
		Vert.	0.166 ± 0.006	0.049 ± 0.008	-0.8 ± 0.8	1 ± 3
	IP5	Hor.	**0.180 ± 0.012**	-0.067 ± 0.012	-2.9 ± 1.7	4 ± 3
		Vert.	0.596 ± 0.002	0.067 ± 0.010	6.1 ± 0.3	14 ± 7
Beam 2	IP1	Hor.	0.638 ± 0.011	0.171 ± 0.018	-0.2 ± 1.5	-5 ± 8
		Vert.	0.158 ± 0.002	-0.024 ± 0.005	0.3 ± 0.2	-1 ± 2
	IP5	Hor.	0.153 ± 0.001	0.018 ± 0.004	0.85 ± 0.15	1 ± 5
		Vert.	0.612 ± 0.002	0.032 ± 0.011	3.7 ± 0.2	-

Table 9: K-modulation measurement results at $\beta^*_{X/||} = 60/15$ cm after global correction. Once again the measurement result of β^*_x shall be discarded for Beam 1 at IP1. The largest mismatch is still observed for Beam 1 at IP5 in the horizontal plane, but got reduced to 20 %.

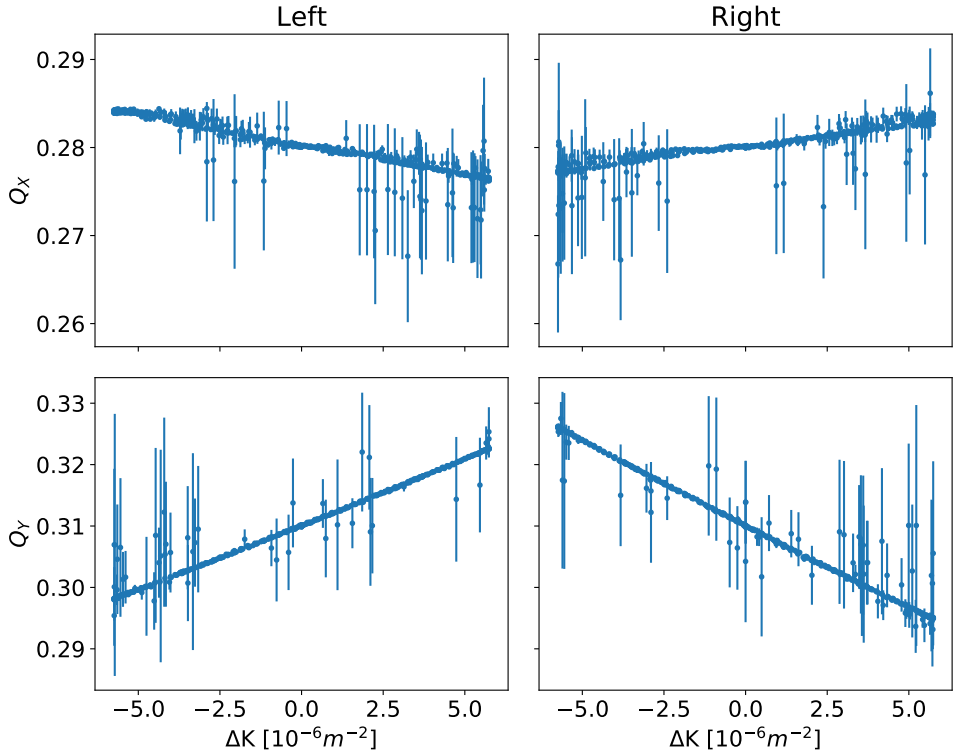

Figure 11: K-modulated tunes measured for Beam 1 after global correction, as a function of the current variations in Q1.L1 and Q1.R1. Once again the horizontal tune signal was of poor quality, spoiling the measurement of β^*_x for Beam 1 at IP1.

4.4 Summary of the flat-optics commissioning shift

Besides the preparation of this new machine configuration for an intensity ramp up, this second test with flat optics was very fruitful, demonstrating the principle of a local optics correction in the

LHC arcs, based on orbit bumps and quadrupolar feed-down effects from the surrounding lattice sextupoles. Applying such a knob to Beam 1, the local β-beating was reduced down to less than 10 % in arc 45, although the exact source of β-beating at mid-arc is still to be explained. Very likely, a similar knob would have been profitable for Beam 2 as well, in view of an incompressible vertical β-beating left at level of 20 % in arc 81 after global correction. The global optics correction of Beam 1 however annihilated a sizable fraction of the former (local) correction in arc 45, which means that the interplay of this new kind of local β-beating knob with traditional optics correction techniques deserves further studies. The final peak β-beating, after all correction trimmed in, was found at the level of 15 % for Beam 1 and 5 % for Beam 2 (except in arc81 where the global correction was unable to bring the peak beta-beating below 20 %).
In one case (B1H in IR1), K-modulation led again to unreliable results that had to be discarded due to lack of consistency with phase advance measurements using the AC-dipole. Within this exception, and an outstanding β^* mismatch of 20 % (B1H in IR5, with 18 cm measured for β_x^* instead of 15 cm), the few percent level (max. 5 %) was demonstrated for both Beams, both IR1 and IR5 and both planes, in the 6 other cases.
All in all, these results certainly announce an increasing difficulty in correcting telescopic optics with large telescopic index ($r^{\mathrm{Tele}} \geq 4$) and/or HL-LHC-like β^* ($\beta^* \lesssim 15$ cm), but a priori no fundamental show stoppers, nor any specific features which could be attributed to flat optics proper.

5 Collimation activities

Collimation activities were conducted in order to validate this new machine configuration for an intensity ramp up. Two fills in MD1 were dedicated to the setting up of the collimation system and to aperture measurements (see also Section 3), whereas the first shift in MD2 was dedicated to the LM campaign for pure validation. Collimator settings (essentially new TCT functions in IR1 and IR5) for this new LHC hypercycle had to be identified and implemented. They were chosen accommodating various requirements:

- for IR3 and IR7 it was decided to keep the 2018 operational functions during the ramp, since a clone of the operational ramp was used;
- minimal corrections to the ramp functions were applied in IR6. Corrections were necessary to accommodate the IR6 optics changes during the telescopic squeeze (which are different between the two beams) without having to change the BETS limits, while achieving similar normalised TCDQ/TCSP settings for the two beams. As presented in Sec. 2.1, the settings of the TCDQ and TCSP of Beam 2 were tightened by 219 μm at the end of the ramp, in order to reach a normalised setting of 7.3 σ at the end of the telescopic squeeze, instead of 7.8 σ which, otherwise, would have left too little margins to accommodate the TCTs of Beam 2;
- Particular care was devoted to the TCTs in IR1 and IR5, since a compromise had to be found between conflicting requirements:
  - Having enough operational margin between TCDQ and TCTs, keeping in mind that the MKD-TCT phase advance was at the acceptance limit (i.e. 30°);
  - Having enough margins between TCTs and the inner triplet, typically $\sim$1 σ;

– Simplicity;

Operationally, the simplest TCT settings are attained at constant gaps in mm. This was (nearly) the case during the pre-squeeze and the telescopic squeeze with a gap carefully adjusted in order to correspond to a normalised aperture of $8.5\,\sigma$ and $8.0\,\sigma$, in the parallel and crossing planes, respectively, at the end of the telescopic squeeze (see Tab. 10). The transition from the end of ramp TCT settings was then deployed during the bump rotation beam process, during which the triplet aperture is not that tight (see Tab. 10). TCT N-σ functions were prepared anyway, using standard commissioning tools, in order to minimise human errors. This implies that in the end the TCT gaps were not strictly constant during the pre- and tele-squeeze, but negligible variations occurred. Table 10 summarizes the deployed collimator settings. The machine aperture as predicted by MAD-X is reported as well for comparison, using the assumptions given in Tab. 11.
These settings were used for all MD2 activities. In MD1, the fill for the optics commissioning and the aperture measurements at β^*=65 cm (see Sec. 3) were run with coarse collimator settings and symmetric TCT settings, as described in Ref. [17], since only pilot bunches were injected.

Family	**Flat top**	**End of Bump Rotation**	**End of pre-squeeze**	**End of tele-squeeze**
TCDQ & TCSP (B1/B2)	7.9/6.9			7.1/7.3
TCT, crossing plane (IR1/IR5)	15	10	9	8.5
TCT, parallel plane (IR1/IR5)	15	15	16	8
aperture, crossing plane (IR1/IR5)	18.4	12.7	10.9	10.4
aperture, parallel plane (IR1/IR5)	17.0	23.0	18.7	8.9
IR7 TCP/TCSG/TCLA	5/6.5/10			
IR3 TCP/TCSG/TCLA	15/18/20			
TCT (IR2/IR8)	37/15			

Table 10: Normalised collimator settings and triplet aperture at 6.5 TeV for the flat-optics hypercycle (taking a reference normalised emittance of 3.5 μm). Settings in IR2, IR3, IR7 and IR8, though not of relevance for beam manipulations at flat-top, are reported for the sake of completeness. The (predicted) triplet aperture is obtained with MAD-X, using the tolerance budget reported in Tab. 11.

Parameter Set	**LHC Measured**
primary halo extension [σ]	6
secondary halo [σ]	6
secondary halo, radial [σ]	6
normalised emittance [μm]	3.5
radial closed orbit excursion [mm]	0.5
momentum offset [10^{-4}]	2
β-beat. fractional beam size change	1.025
relative parasitic dispersion	0.1

Table 11: Parameters used for the generic calculation of the machine aperture with MAD-X [18].

5.1 Aperture measurements

Aperture measurements were carried out in the second shift of MD1 (see Sec. 3). The time allocated to the MD was not enough to have a thorough aperture measurement, as done during the standard machine commissioning at the beginning of each running year. Hence, measurements were aimed at simply checking that the machine aperture was beyond the cut provided by TCTs. The method was to take loss maps while gradually increasing the TCT opening. The moment when losses move from the TCTs to the triplet determines the measured aperture. The procedure started with the TCTs centered around the beam. The collimators were opened in steps of 0.5 σ, and the usual set of four betatron loss maps was taken.
Fill 6814, with only pilots, was dedicated to measurements at β^*=65 cm. The TCT starting position was 10 σ. Fill 6815, with two nominal bunches (for finding collisions) and some pilots, was dedicated to measurements at β^*=60/15 cm. The TCT starting position was 9 σ.
Table 12 reports the aperture measurements. As it can be seen, the LHC aperture was found to be safely outside the necessary margins beyond TCT settings.

β^* [cm]	**B1H** [σ]	**B1V** [σ]	**B2H** [σ]	**B2V** [σ]
65	>13			
60/15	>9.5	9.5-9.8 (Q3R1)	>9.5	>9.5

Table 12: Summary of aperture measurements taken with the flat ATS optics. Apertures are indicated in normalised values, referred to a normalised emittance of 3.5 μm.

5.2 TCT centre functions

Dedicated TCT centre functions were prepared in view of the activity with trains. The alignment campaign took place in the second flat-optics shift of MD1, with fill 6815 (see Sec. 3) where two nominal bunches per beam were injected. The TCTs were aligned at each stop between the different beam processes deployed at flat-top energy, namely the bump rotation, pre-squeeze, tele-squeeze and physics beam processes. To be noted, that TCT centre functions based on pure MAD-X predictions (starting from the last point of the energy ramp) were computed as well as a starting point for the aperture measurement campaign (fill 6814 and 6815), but they were not re-used afterward.

As an example, Figs. 12 and 13 show the TCT centre functions in IR1 and IR5, respectively, during the bump rotation beam process.

5.3 Loss maps

A first set of loss maps was taken already in fill 6815 (see Sec. 3), at the end of the tele-squeeze beam process, right before going to collision. The aim of the LMs was to verify that the choice of asymmetric settings among planes (e.g. 8/9 σ) did not show any immediate drawback. LMs were taken after quickly centering the TCTs thanks to the BPM-based alignment.
The full LM campaign was actually carried out in the first flat-optics shift of MD2. Because of the limited time allotted in MDs, only betatron LMs were taken, at the end of the bump rotation, pre-squeeze and tele-squeeze beam processes, and in collision. An additional set of betatron LMs was taken with the half-crossing angle decreased to 100 μrad, in order to also validate the machine at

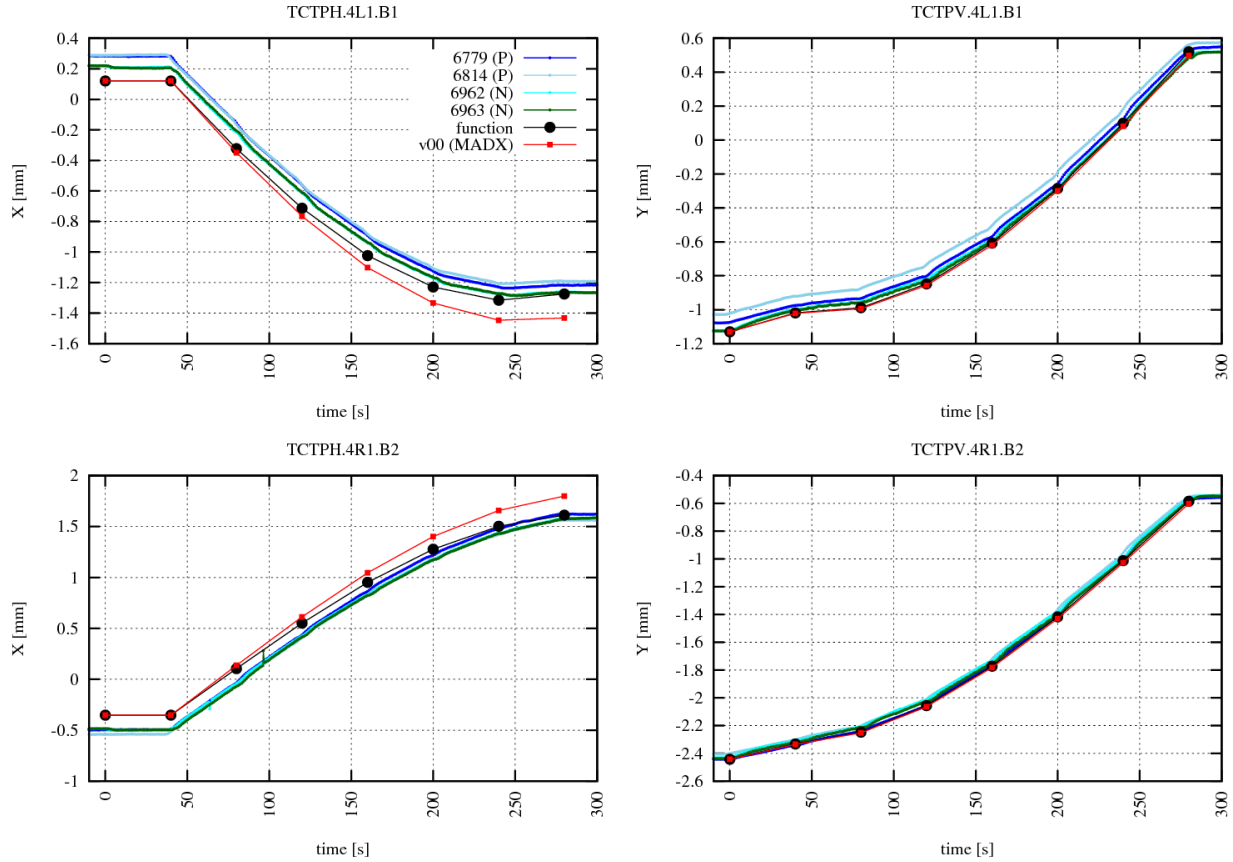

Figure 12: IR1 TCT centre functions during the bump rotation beam process. Black points show the functions based on alignment data, whereas the red squares mark those based only on MAD-X predictions (preliminary). Other colors correspond to measurements taken during the indicated fills ("P": fills with pilot bunches; "N": fills with nominal bunches).

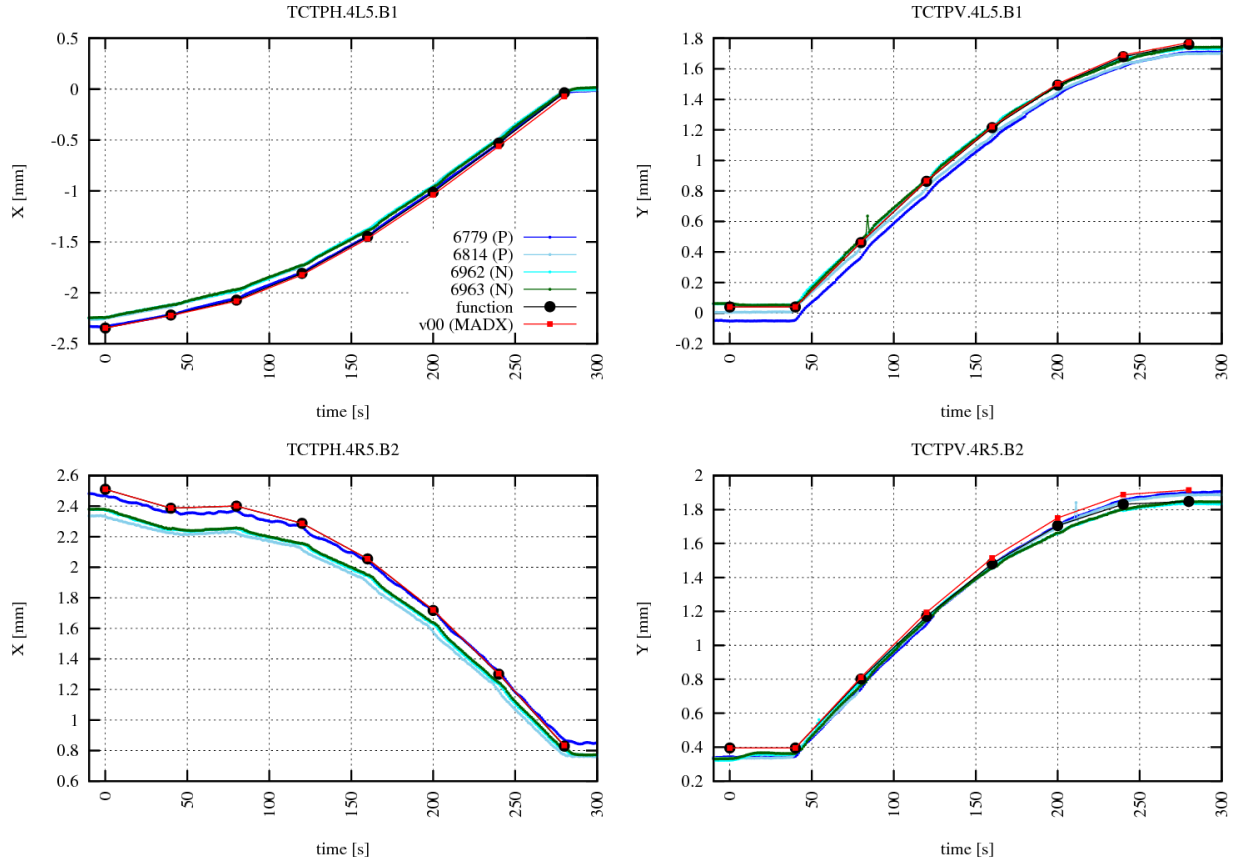

Figure 13: IR5 TCT centre functions during the bump rotation beam process. Black points show the functions based on alignment data, whereas the red squares mark those based only on MAD-X predictions (preliminary). Other colors correspond to measurements taken during the indicated fills ("P": fills with pilot bunches; "N": fills with nominal bunches).

reduced crossing angles. An asynchronous beam dump test was done after the last betatron LMs in collision (with the half-crossing angle re-increased to $130\,\mu$rad). The results obtained were found OK by the team in charge.

As an example, Fig. 14 shows the betatron LMs taken in collision with an half-crossing angle of $130\,\mu$rad. All LMs show a peak of up to 10^{-4} at the Q3 of IR1 on the incoming beam side, with the upstream TCT at 10^{-3}, hinting to a possible leakage from the tertiary collimator. Other recurrent peaks are found in cells 16L1 and 24L1 for B1H and B1V, of the order of some 10^{-5}. A peak is also found in cell 13R8 at 2×10^{-5}. None of these peaks was found to be problematic for allowing tests with trains, but they should be understood in simulations. It should be noted that the peak in 16L1 was also observed in the LMs taken at β^*=65 cm, which is not the case for the other peaks mentioned above. For all LMs taken, the collimation hierarchy in IR7 did not show any particular anomaly, with a local inefficiency of the order of 10^{-4} in the dispersion suppressor (see the zoom of IR7 in Fig. 15 for the betatron LMs taken in collision).

5.4 Summary of the collimation

Collimation activities in support to the flat-optics MDs were focused on the generation and implementation of collimator settings and functions, in order to allow tests with trains. While the 2018 operational functions were kept for the energy ramp (with only minor changes in IR6 to avoid too different settings between the two beams), dedicated TCT N-σ and centre functions were successfully implemented, in particular to allow the complex crossing bump gymnastics in IR1 and IR5, and the new subsequent machine configuration with flat optics, while keeping the machine safely protected all along. The triplet aperture was found slightly larger than expected at $\beta^*_{X/||} = 60/15$ cm. Qualification LMs finally showed that the machine was adequately protected against risks of quenches with trains, and the green light was given for an intensity ramp up.

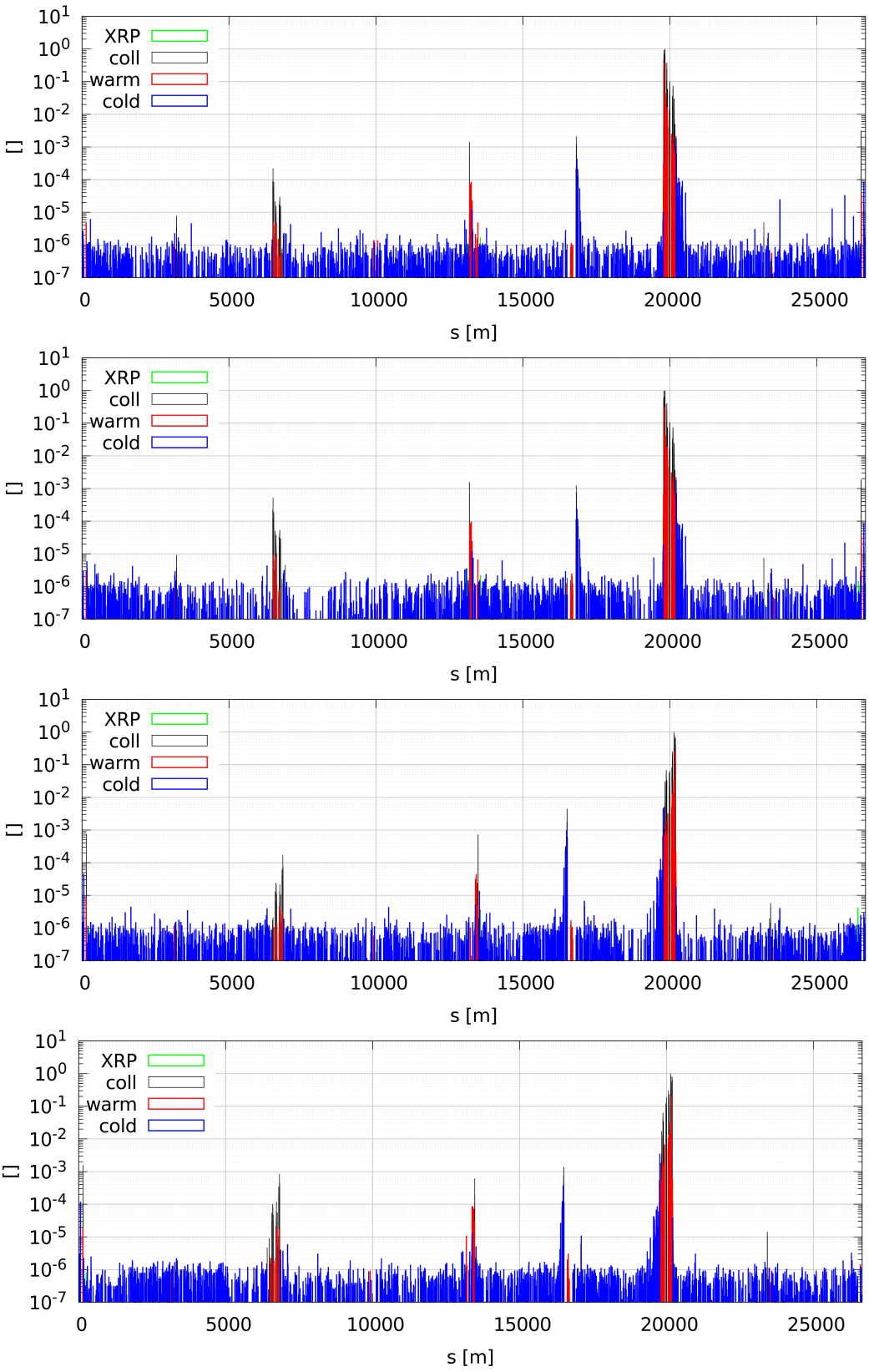

Figure 14: Qualification loss maps with colliding beams. From top to bottom: B1H, B1V, B2H and B2V. The entire LHC ring is shown.

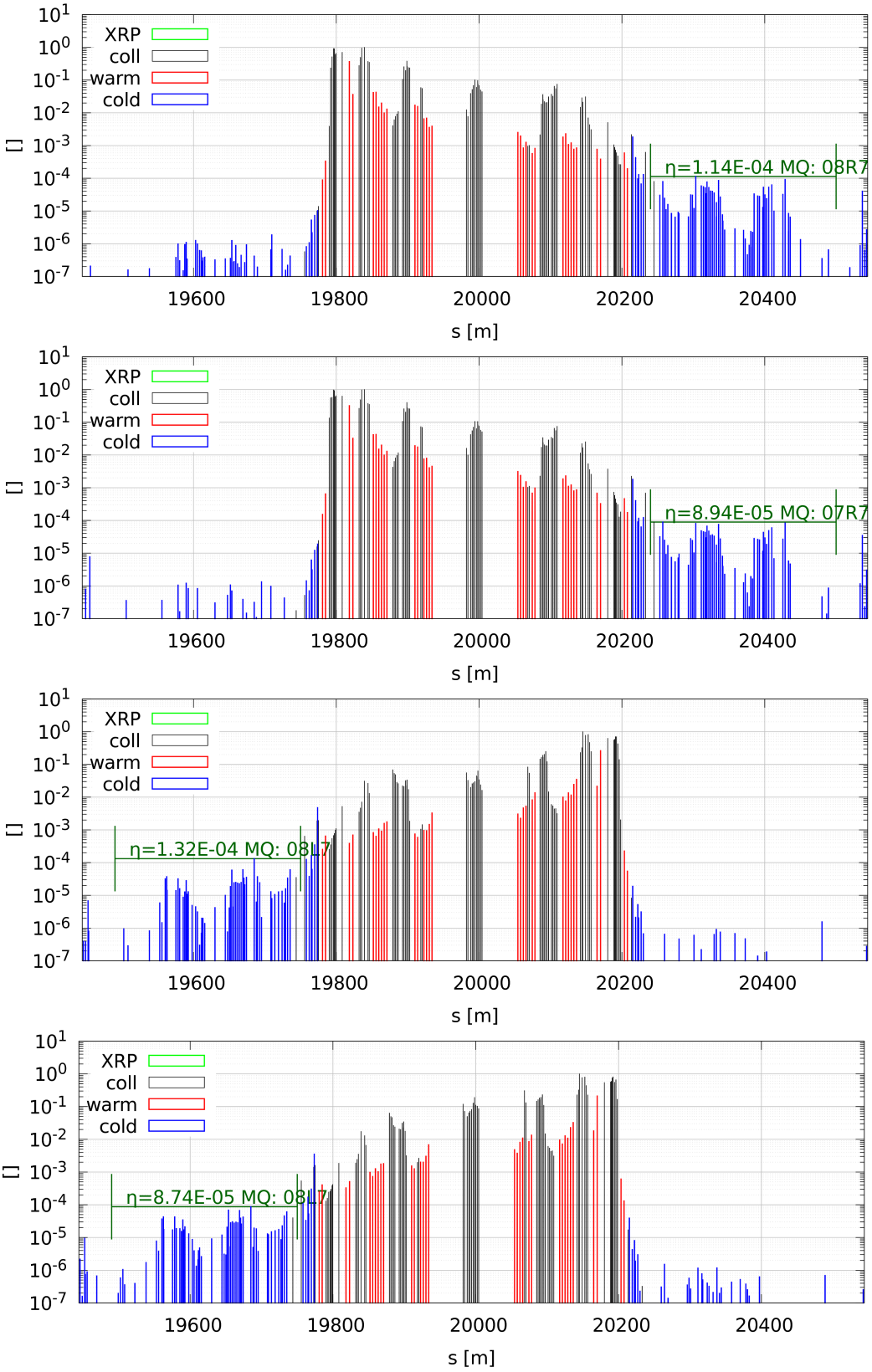

Figure 15: Qualification loss maps with colliding beams. From top to bottom: B1H, B1V, B2H and B2V. The zoom on IR7 is shown.

6 High-intensity beam tests

6.1 Filling scheme

For the high-intensity test, the machine was filled with 61 nominal bunches, namely: one non-colliding bunch (INDIV) for tune monitoring, and 12b + 48b (BCMS) colliding only in IR1 and IR5, with no long-range beam-beam (BBLR) interactions in IR2 and IR8 (see Fig. 16). The spacing between the 3 SPS injections was also maximized in order to prevent from any BBLR interactions in IR1 and IR5, between the INDIV and the 12 bunch train, and between the 12 bunch train and the BCMS train.

RFBucket	Bu Tot	bu/btch	Spc/ns	PSbchs	I level	RFBucket	Bu Tot	bu/btch	Spc/ns	PSbchs	I level
1	1	1	0	1	NOM	*311*	1	1	0	1	NOM
711	12	12	25	1	INTR	*711*	12	12	25	1	INTR
1221	48	48	25	1	NOM	*1221*	48	48	25	1	NOM

Figure 16: Filling scheme.

6.2 Beam lifetime

The injection and (nominal) ramp beam processes were smooth, together with the EoR knob gymnastics described in Section 2.2 (standard to `TELE` knobs exchange, and tune change). The beam lifetime evolution during the crossing bump gymnastics is illustrated in Fig. 17, showing large fluctuations in relative for both beams (in particular an improvement for Beam 1 at $45°$, and conversely for Beam 2), but nothing really dramatic in terms of minimum lifetime ($\gtrsim 100$ h during the overall beam process). On the other hand, Beam 2 suffered from an horizontal instability which started to develop in the crossing bump rotation beam process, and then continued in the first segments of the pre-squeeze (see Section 6.5), leading essentially to an emittance growth with only very mild losses.

The beam lifetime evolution during the pre-squeeze and subsequent telescopic squeeze did not reveal either any striking features, except, as usual, a net reduction towards the end of the squeeze (EoS) down to about 100 h in absolute for the final optics at $\beta^*_{X/\|} = 60/15$ cm (see Fig. 18). To be noted that an instability was also observed, this time for Beam 1 in the vertical plane, when the octupole current was approaching 200 A towards the end of the telescopic squeeze (see Section 6.5). This explains the negative spike of life time down to 10 h for Beam 1 in Fig. 18, which can be observed just before the end of the squeeze.

A very poor lifetime of ~ 12 h for both beams was however observed as soon as the first collisions were established and optimized. The MO polarity was first immediately reverted. Then, following a tune re-optimization, essentially along the diagonal ($\Delta Q_{x,y} \sim +0.004$ leading to a final working point of .321/.327, see Section 2.5), a more decent lifetime of 20-21 h was recovered, with no unbalance between Beam 1 and Beam 2 (see Fig. 19), and found to correspond to the burn-off limit, at least for Beam 1 (see Section 6.5).

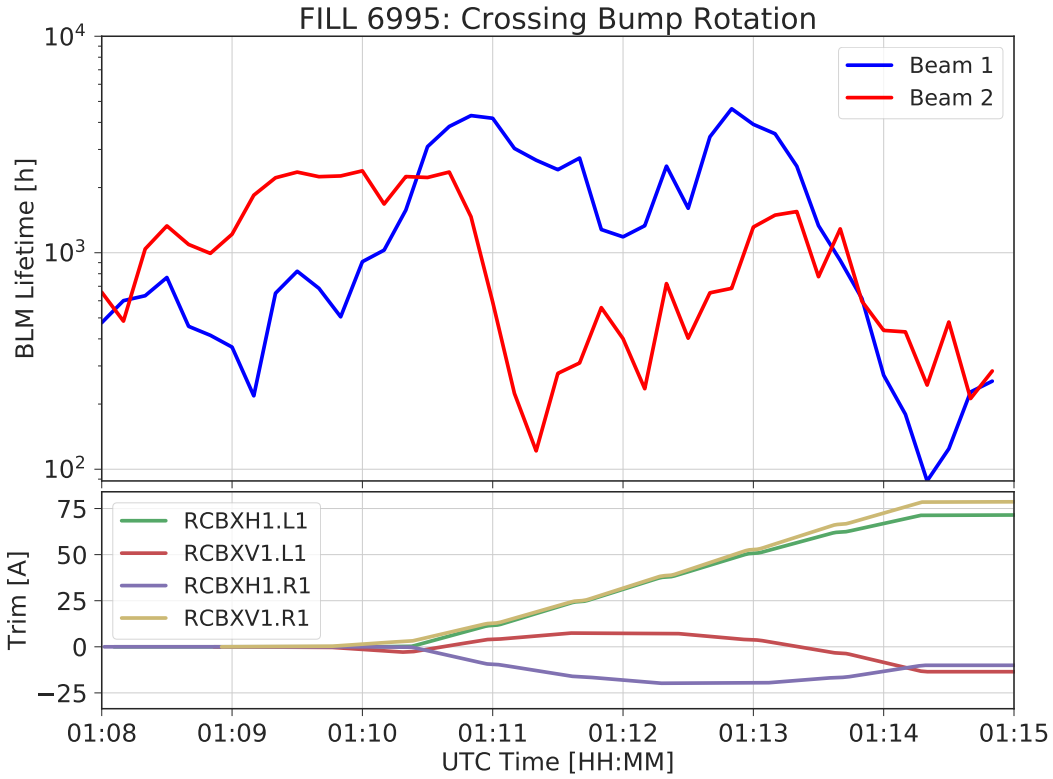

Figure 17: Beam lifetime evolution during the crossing bump rotation (main plot), and setting evolution of the MCBX corrector (bottom plot). At the beginning of the beam process, the crossing angle is first slightly reduced from $160\,\mu$rad down to $150\,\mu$rad in IR1 and IR5, at constant parallel separation (± 0.55 mm). The rotation then deploys an horizontal (resp. vertical) crossing angle in IR1 (resp. IR5), together with a vert. (resp. horiz.) parallel separation. For a given plane, and on a given side of the IR, the crossing angle and parallel separation variations add up in terms of corresponding MCBX current variations (case of RCBXH1.L1 and RCBXV1.R1) while they partially compensate on the other side of the IR (case of RCBXH1.R1 and RCBXV1.V1). This is due to the fact that the MCBX matrix coefficients of the crossing knob are left/right antisymmetric, while they are symmetric for the parallel separation knob.

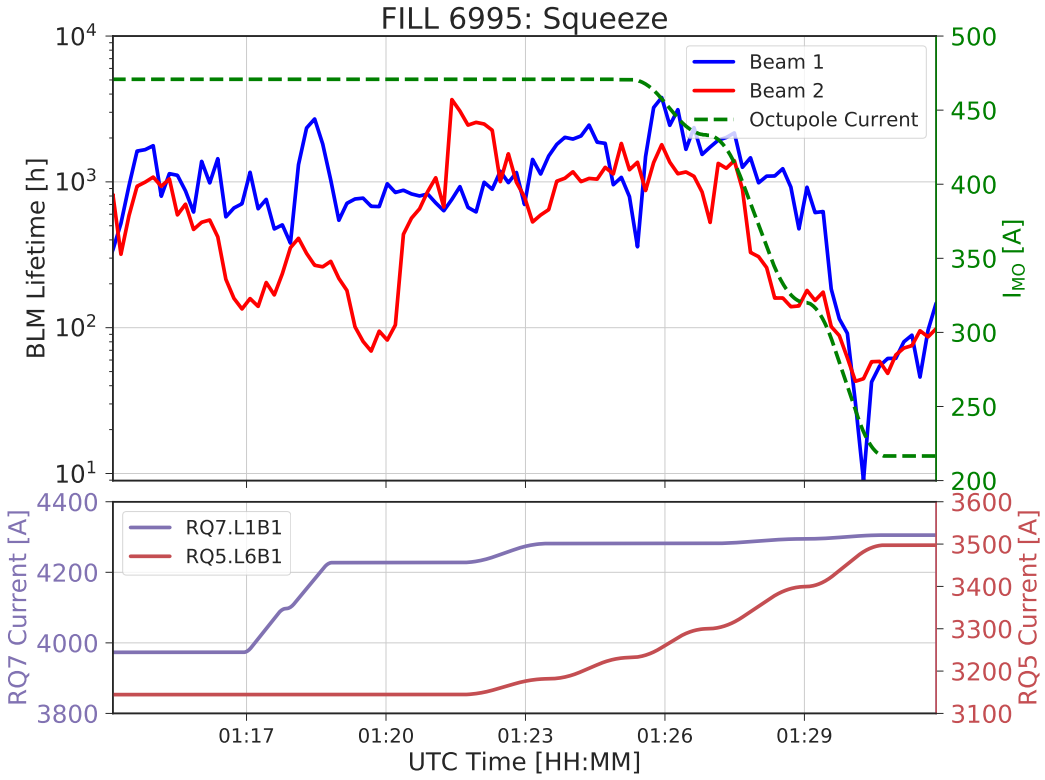

Figure 18: Beam lifetime evolution during the pre-squeeze and telescopic squeeze (main plot), with the MO current superimposed. The bottom plot is just the signature of these two beam processes where the current of Q7.L1B1 is changing during the pre-squeeze (3 matched points, see Tab. 1), then remains (quasi-)constant during the tele-squeeze (within the β-beating correction knob variations, and the small pre-squeeze continuation from 65 cm down to 60 cm which is combined with the first tele-squeeze segment, see Tab. 2), and conversely for the Q5.L6B1 current (constant during the pre-squeeze, and changing during the tele-squeeze).

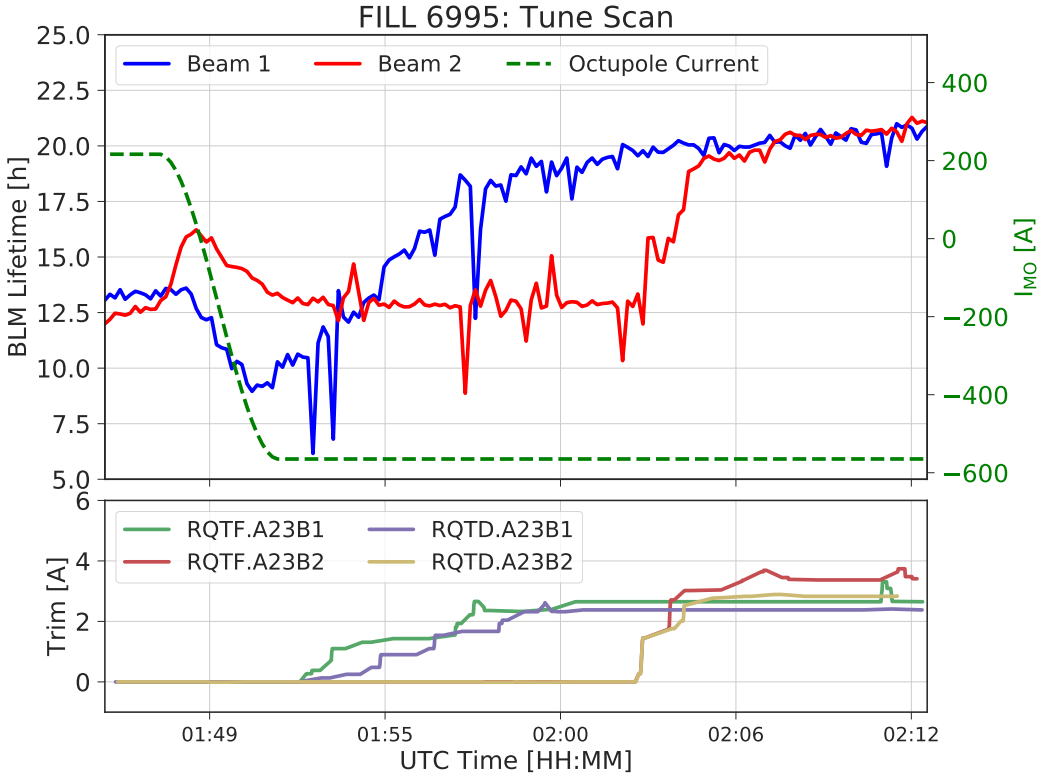

Figure 19: Beam lifetime recovery in collision by shifting up the tune by $\Delta Q_{x,y} \sim 0.004$ along the diagonal, implemented by steps for Beam 1, and in one go for Beam 2.

6.3 Luminosity and co-linearity knobs

After optimization, the peak luminosity was approaching 5×10^{32} cm^{-2} s^{-1} for 60 colliding bunches (61 bunches in total), with an average population of $\langle N_p \rangle = 1.04 \times 10^{11}$ p/b (see Fig. 20). For a sake of comparison, it is worth noting that a typical peak luminosity of 2×10^{34} cm^{-2} s^{-1} for the 2018 proton run at beginning of stable (2548 colliding bunches with $\sim 1.15 \times 10^{11}$ p/b) corresponds to about $\sim 3.8 \times 10^{32}$ cm^{-2} s^{-1} for the MD beam parameters, that is almost 25 % less than the luminosity published in Fig. 20.

Several studies then followed to investigate the crossing angle reach in this non-nominal configuration with flat optics (see Section 6.4). Before dumping the beam a special knob, the so-called collinearity knob, was tested to fine tune the luminosity in ATLAS and CMS (one knob per insertion). This knob was designed to act anti-symmetrically on the powering of the left and right skew quadrupole corrector magnets of the triplets in IR1 and IR5 (MQSX), with 1 unit in knob value corresponding to a trim by $\delta K = \pm 10^{-4}$ m^{-2} for the normalised strength of the left and right MQSX magnets hosted in a given experimental insertion. Since (for round optics), the B1H, B1V, B2H and B2V β-functions are by design nearly the same at the MQSX position, and assuming a good enough β-beating correction in the machine, the knob was not expected to impact on the global coupling (regardless of the optics), while inducing a sort of closed coupling bump with maximal amplitude at the IP, the same amplitude for both beams but with an opposite phase between Beam 1 and Beam 2. For flat optics, it means that acting on this knob can a priori help

28-Jul-2018 03:45:37	Fill #: 6995	Energy: 6499 GeV	I(B1): 6.32e+12	I(B2): 6.36e+12
	ATLAS	ALICE	CMS	LHCb
Experiment Status	STANDBY	STANDBY	STANDBY	STANDBY
Instantaneous Lumi [(ub.s)^-1]	480.230	0.000	495.734	0.011
BRAN Luminosity [(ub.s)^-1]	609.8	0.0	432.8	0.0
Fill Luminosity (nb)^-1	0.000	0.000	0.000	14979.054
Beam 1 BKGD	0.000	0.000	2.324	0.000
Beam 2 BKGD	0.000	0.000	0.890	0.021
Beta*	0.65 m	10.00 m	0.65 m	3.00 m
Crossing Angle (urad)	0(V)	200(V)	0(H)	-250(H)
LHCb VELO Position	OUT	Gap: -0.0 mm	ADJUST	TOTEM: CALIBRATION

Figure 20: First collisions of trains with flat optics in the LHC ($\beta^*_{X/\|\|} = 60/15$ cm with an half-crossing angle of 130 μrad). The luminosity is approaching 5×10^{32} cm^{-2} s^{-1} in ATLAS and CMS for 60 colliding bunches (61 bunches in total) with an average population of $\langle N_p \rangle = 1.04 \times 10^{11}$ p/b.

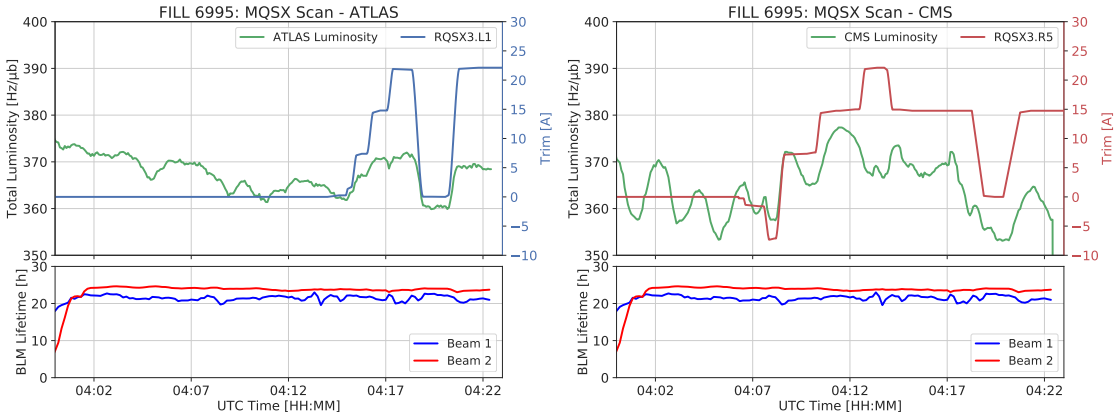

Figure 21: Lumi scan in ATLAS (left) and CMS (right) acting on the corresponding collinearity knob.

in finding the best possible transverse overlap of the two beam ellipses at the IP (and de facto the maximum possible luminosity). In all cases, such a knob enables a fine tuning of the left and right skew quadrupole correction of the inner triplet (e.g. in case of local coupling left over after any optics commissioning campaign). The corresponding ATLAS and CMS lumi scans are shown in Fig. 21, which indeed demonstrated a possible improvement of the luminosity by up to 3-4 % by acting on this knob in IR1 and IR5 (+1.5 units at IP1, and -1.0 unit at IP5), with no detrimental impact on the beam lifetime.

In another context, during the 2018 ion Run, the hazard made that this knob was also tried out in IR2, as a potential remedy to boost the luminosity in Alice which was found dramatically lower than expected after the very first ion physics fills. Trimming this knob by up to ~ 12 units (compared to a fine tuning level of about 1-2 units) fully restored the luminosity in Alice. Based on this observation, in depth investigations concluded that indeed the strengths of the left and right skew quadrupole correctors in IP2 were swapped by mistake during the machine setup phase [19].

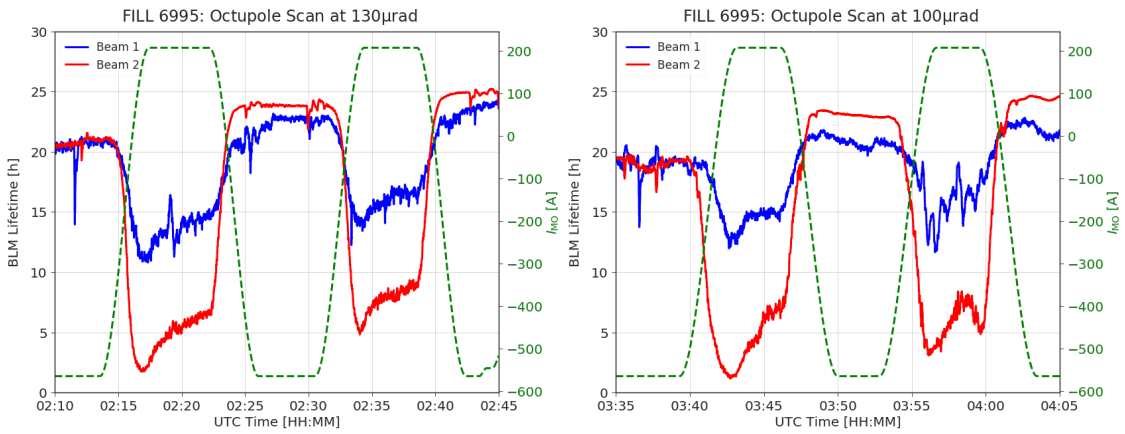

Figure 22: Correlation between beam lifetime and octupole with a half-crossing angle of 130 μrad (left) and 100 μrad (right).

6.4 BBLR mitigation with octupoles

With the beams colliding, two scans in octupole current took place, the first one with a half-crossing angle of 130 μrad (corresponding to a normalised crossing angle of $10.6\,\sigma$ with $\beta^* = 60$ cm in the crossing plane and a normalised emittance of $\gamma\epsilon = 2.5$ μm), and the second MO scan with 100 μrad ($8.2\,\sigma$). The average bunch population was in the range of 10^{11} p/b for the first scan, and in the range of 0.9×10^{11} p/b for the second scan. In both cases the correlation between beam lifetime and octupole currents is striking in Fig. 22, confirming for flat optics as well, the potential mitigation of the BBLR interactions by using the lattice octupole with negative polarity. It is important to stress that during these scans Beam 1 was systematically found to be much more robust than Beam 2, contrary to what was generally observed during the 2018 luminosity run (with nominal round optics and V/H crossing angle in IR1/5). Looking at the bunch by bunch data, more specifically at the burn-off subtracted life time of a few selected bunches, the above observation was confirmed, and precisely quantified in terms of extra-losses with respect to the burn-off limit (see Fig. 23 and Fig. 24 for the two MO scans at 130 μrad and 100 μrad, respectively).

Concerning Beam 1, the first MO scan (130 μrad with an average bunch population of 10^{11} p/b), demonstrated the burn-off limit (80 mb) for all selected bunches when reverting the MO polarity and pushing the current down to -570 A [see Figs. 23(a)-(b)]. From the second MO scan, the half crossing angle of 100 μrad was found slightly beyond the acceptable limit, at least for the so-called regular bunches experiencing the maximum possible number of BBLR encounters [see Figs. 24(b)], but not necessarily for 12 bunch train [see Figs. 24(a)], and/or the so-called intermediate and pacman bunches of the BCMS train (with three quarters or only half of the BBLR encounters).

Concerning Beam 2, the half-crossing angle of 130 μrad was probably already at the limit for the regular bunches [see Fig. 23(d)], probably due to the large emittance which followed the B2H instability during the crossing bump rotation (see Section 6.5). In general, however, the Beam 2 sensitivity to the MO current variations was found extremely large, even for the 12 bunch train [see Figs. 23(c) and 24(c)]. This effect is attributed to some net correlations which were identified a posteriori between octupole current and vertical tune, sensibly more for Beam 2 (see Fig. 25).

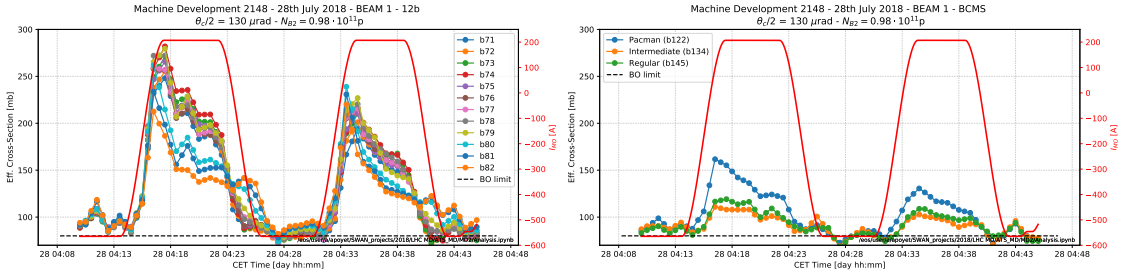

(a) Beam 1: 12 b train

(b) Beam 1: BCMS train

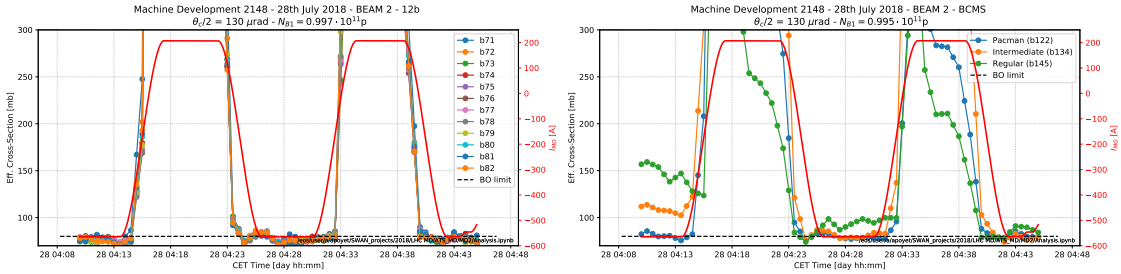

(c) Beam 2: 12 b train

(d) Beam 2: BCMS train

Figure 23: MO scan in collision with a half-crossing angle of 130 μrad in IR1 and IR5 ($\langle N_p \rangle \sim 10^{11}$ p/b): effective cross-section (i.e. loss rate normalised to luminosity) of individual bunches selected in the 12 bunch (left) and BCMS (right) trains of Beam 1 (top) and Beam 2 (bottom).

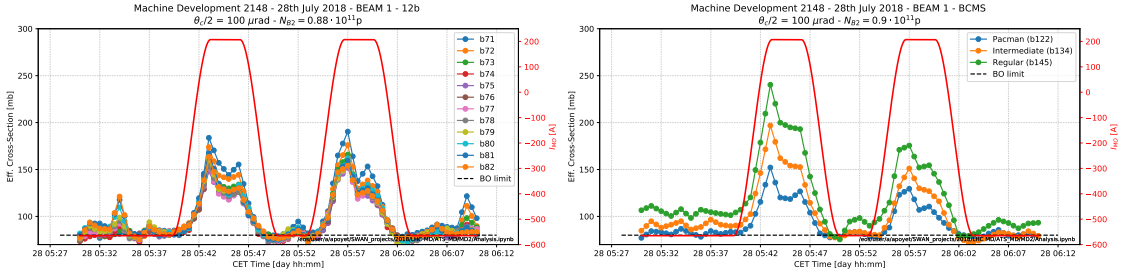

(a) Beam 1: 12 b train

(b) Beam 1: BCMS train

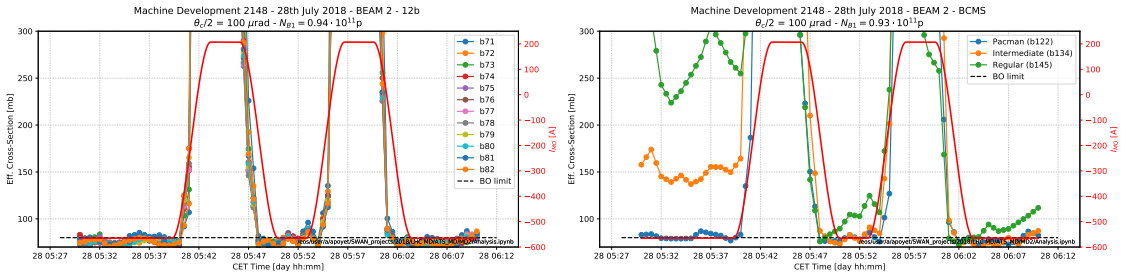

(c) Beam 2: 12 b train

(d) Beam 2: BCMS train

Figure 24: MO scan in collision with a half-crossing angle of 100 μrad in IR1 and IR5 ($\langle N_p \rangle \sim 0.9 \times 10^{11}$ p/b): effective cross-section (i.e. loss rate normalised to luminosity) of individual bunches selected in the 12 bunch (left) and BCMS (right) trains of Beam 1 (top) and Beam 2 (bottom).

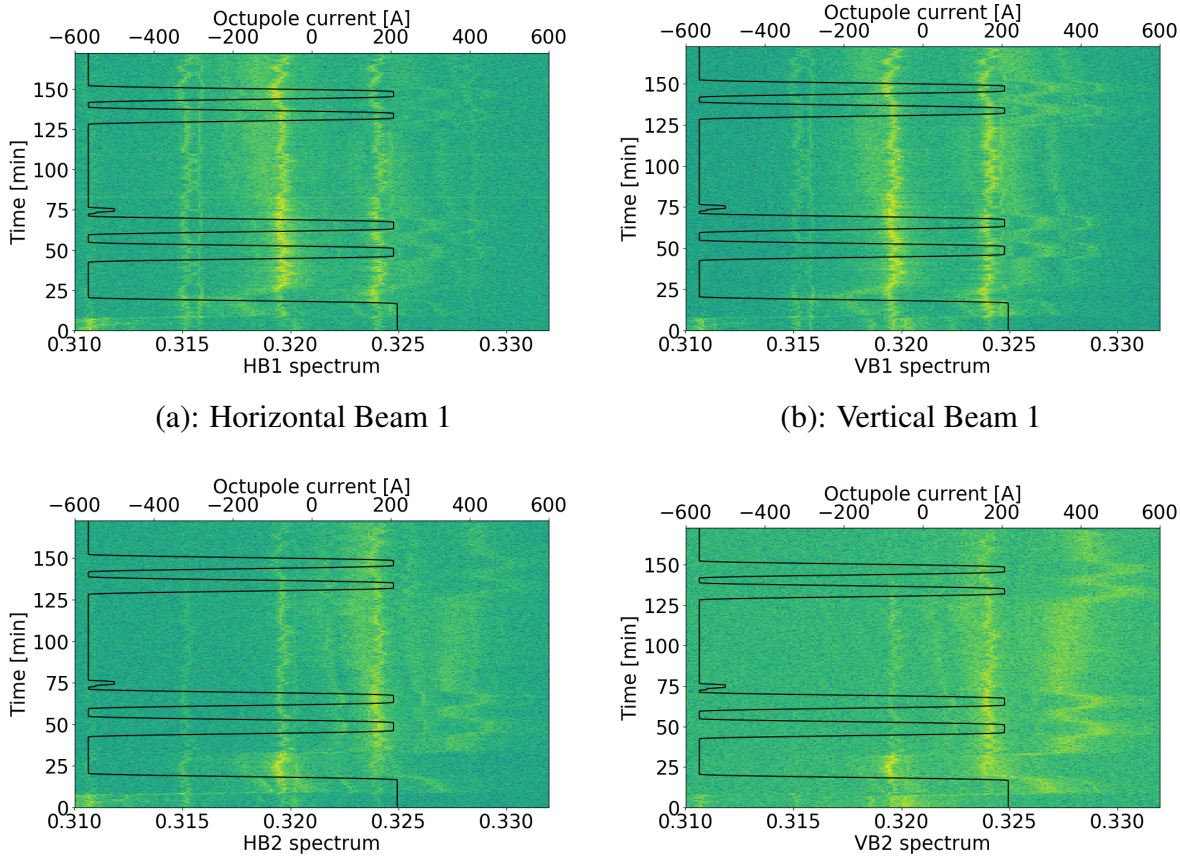

(a): Horizontal Beam 1

(b): Vertical Beam 1

(c): Horizontal Beam 2

(d): Vertical Beam 2

Figure 25: Spectrogram of the beam oscillation amplitude measured by the BBQ gated on the first non-colliding bunch of each beam, with the octupole current superimposed. The time $t = 0$ coincides with the start of the collision beam process. The signal is dominated by two brighter lines due to external noise (at $Q_{x/y} \sim 0.320/0.324$). The tune lines actually correspond to the ones showing some correlations with the octupole currents, around $Q_{x/y} \sim 0.32/0.325$ for Beam 1 and $Q_{x/y} \sim 0.323/0.327$ for Beam 2, after a net shift which is visible in the first few minutes, and coming from (i) a first tune shift of $\Delta Q_{x/y} = 0.007/0.003$ which was preset in the collision BP (see Section 2.5), followed immediately by an additional tune shift of $\Delta Q_{x/y} = 0.004/0.004$ for life time optimization (see Section 6.2 and Fig. 19). As a consequence, the horizontal tune line of Beam 1 is hardly visible, being very close to one of the two noise lines [see Fig. (a)]. While the tune changes from the MO current variations are very mild in the horizontal plane [hardly more than a few 10^{-4}, see e.g. B2H in Fig. (c)], a net effect is visible in the vertical plane, sensibly more for Beam 2 (up to $\sim 2 \times 10^{-3}$). For positive MO polarity (MO powered with + 200 A), this correlation brought the non-colliding bunch of Beam 2 very close to the third order resonance, and similarly for the colliding bunches of both beams, but to more or less extent, depending on their individual BBLR induced tune shift which is negative.

6.5 Observation of instabilities

Two instabilities were detected over the cycle, the first one in the horizontal plane of Beam 2 during the second half of the crossing bump rotation, and the second one, milder, in the vertical plane of Beam 1 during the last step of the telescopic squeeze. The beam oscillation spectrograms are shown in Fig. 26.

Concerning the first instability B2H, the activity of individual bunches at the end of the crossing bump rotation and beginning of the pre-squeeze is shown in Fig. 27-(a). The instability starts at the third last step of the crossing bump rotation, initially with one bunch located at the head of the BCMS train, and then affecting trailing bunches within the next minutes. Based on a linear chromaticity of $Q' = 10$ (see Section 2.6.4), and on the measured beam parameters (in particular $\gamma\epsilon_y \sim 1.5\,\mu$m in the vertical plane[3], see Fig. 28), the theoretical instability threshold for these bunches is about 295 A, corresponding to 590 A when including the empirical factor of 2 found to be needed in operation. The octupole current was 471 A, to which an equivalent of ≈50 to 100 A can be added depending on the position of the bunch in the train, due to the long-range beam-beam interactions. During the rotation of the crossing bump, skewed BBLR interactions introduce a linear coupling reaching $|c^-| \approx 2 \times 10^{-3}$ for the central bunches (half for the extreme pacman bunches). This does not seem sufficient to explain the instabilities observed. However this contribution might have added up to other sources of linear coupling, e.g. through feed down effects from the non-linear field imperfections of the inner triplets (with no pre-settings given to the MCSX and MCSSX magnets, see Section 2.3). In this respect, the execution of the crossing bump rotation with a larger fractional tune split would be advisable. In practice, this means to run the Q-change beam process after the crossing bump rotation, and not before as this had been designed for the MD (see Section 2.2). The instability was quite strong, with no dramatic losses, but a severe emittance growth observed on several bunches (see BSRT snapshot taken after the instability in Fig. 28).

Concerning the B1V spectrogram in Fig. 26-(c), the apparent activity on the bottom of the picture is just the result of cross-talks with the instability B2H of above through the BBLR interactions. On the full spectrograms of both beams [Figs. 26-(a) and 26-(c)], it is then worth noting a negative frequency shift developing towards the end of the telescopic squeeze, whereas the gated system sees a straight tune [Figs. 26-(b) and 26-(d)]. This shift is attributed to the uncompensated tune shift along the diagonal induced by the long-rang beam-beam interactions with flat optics[4]. The instability in the vertical plane of Beam 1 is then visible on the top of Fig. 26-(c), with intermediate frequencies showing up, in between the unperturbed tune measured by the gated system [Fig. 26-(d)] and the BBLR shifted tune dominated by the full beam signal. This is consistent with the single bunch activity showing that the instability only affected pacman bunches at the end of the train [Fig. 27-(b)]. Compared to the central bunches, the pacman bunches are indeed the most critical ones in terms of beam stability when the octupole polarity is set to positive. Nevertheless, as shown in Fig. 29, these bunches were actually expected to be stable, even for an emittance

[3] When the octupole polarity is positive, the Landau damping mechanism is driven by the cross-anharmonicity term, which means that the vertical emittance is the relevant parameter entering into the beam stability in the horizontal plane, and conversely for the horizontal emittance.

[4] A fraction of this BBLR induced tune shift was compensated during the collision BP (see section 2.5), and another fraction when optimizing the beam lifetime in collision (see Fig. 19). Ideally this shift should be compensated as soon as it becomes significant towards the end of the telescopic squeeze, with some good compromise to be found between regular and pacman bunches.

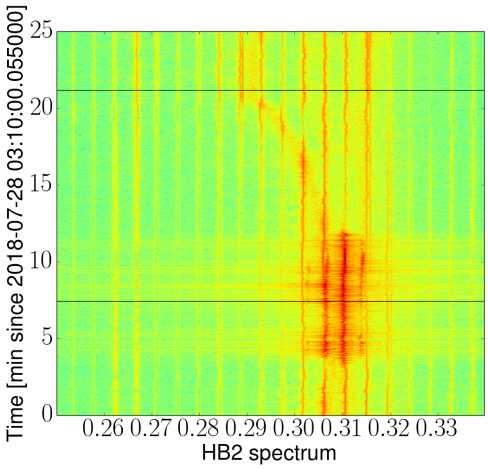

(a): Horizontal Beam 2, High sensitivity

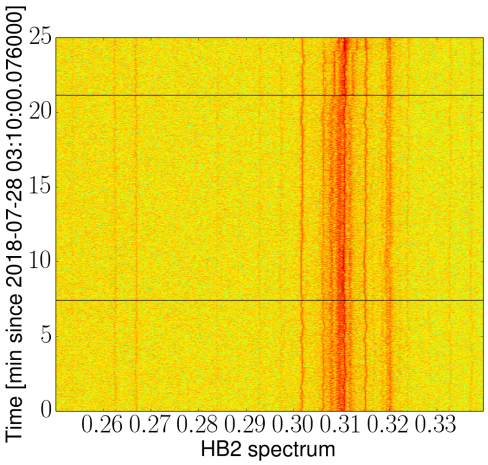

(b): Horizontal Beam 2, Gated

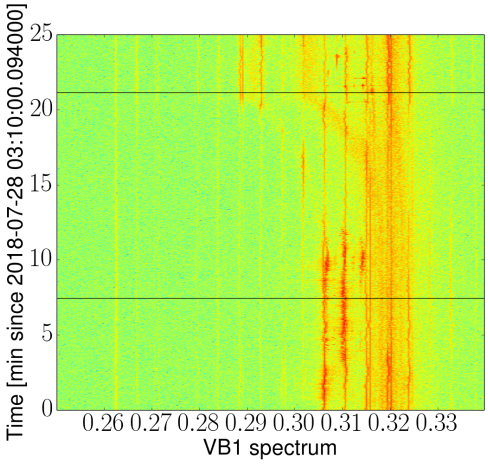

(c): Vertical Beam 1, High sensitivity

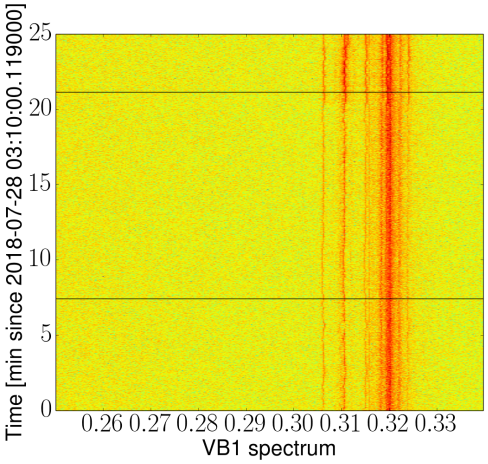

(d): Vertical Beam 1, Gated

Figure 26: Spectrogram of the beam oscillation amplitude measured by the BBQ. Whereas the high sensitivity system measures all bunches in the beam (left pictures), the gated system measured the first non-colliding bunch of each beam (right pictures). The black horizontal lines mark the start and end of the beam mode SQUEEZE, which includes the pre-squeeze and telescopic squeeze BPs. Note the shift by 2 h between the local time used in these pictures, and the UTC time in Figs. 17 and 18.

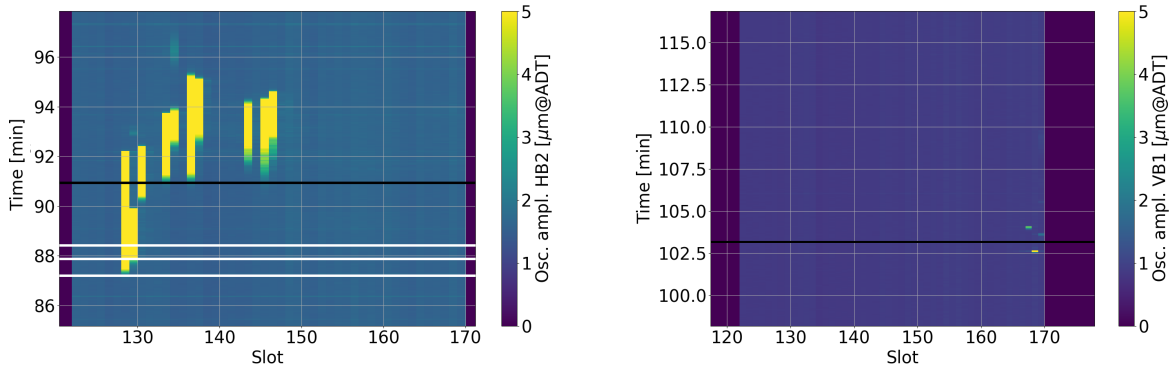

(a): Horizontal Beam 2

(b): Vertical Beam 1

Figure 27: Transverse oscillation amplitude of individual bunches measured by the ADT activity monitor during the two instabilities observed. The start and end of the beam mode SQUEEZE are marked with the black horizontal line on the left and right plot, respectively. The last three matched points of the crossing bump rotation are marked with white the horizontal lines on the left picture.

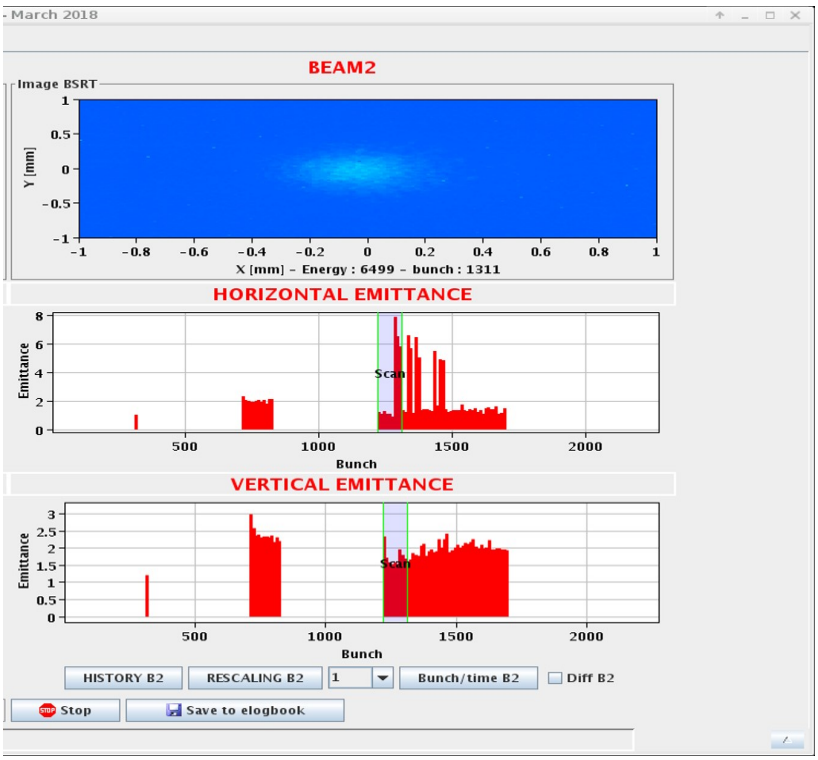

Figure 28: BSRT snapshot taken for Beam 2 after the B2H instability. The BSRT was unfortunately not properly reset for Beam 1, which explains the absence of emittance data for Beam 1 during the MD period.

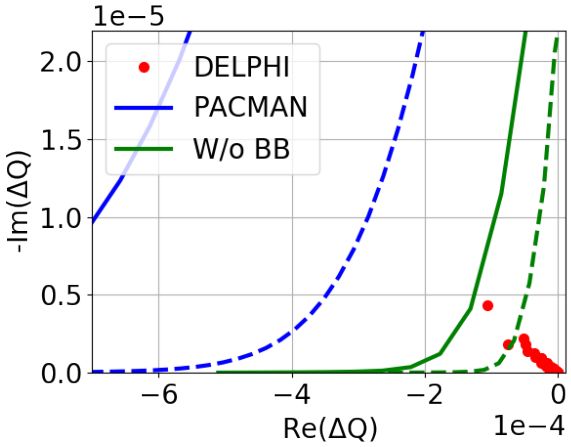

Figure 29: Stability diagram at the end of the telescopic squeeze (MOs powered with 215 A), as obtained numerically from MAD-X tracking and PySSD, together with the coherent tune shifts calculated with DELPHI, assuming $Q' = 10$ and the nominal 2018 configuration (e.g. the small impact from the non-nominal TCT settings is not taken into account). A bunch population of 1.1×10^{11} p/b within a normalized emittance of 1 μm is considered. The dashed lines accounts for the empirical factor 2 in the estimate of the instability threshold. The pacman bunches were actually expected to be stable, thanks to the BBLR induced tune spread at $\beta^*_{X/||} = 60/15$ cm with a half-crossing angle of $130\,\mu$rad.

as small as $\gamma\epsilon_x = 1\,\mu$m, due to the quite large BBLR induced tune spread with a half-crossing angle of $130\,\mu$rad. On the other hand, assuming a similarly small emittance for the non-colliding bunch, the latter should have been be unstable with the octupole powered to only 215 A at the end of the tele-squeeze. This second (and milder) instability is therefore not yet understood at this stage. As already discussed in Section 2.6.5, a less aggressive reduction of the MO current in the tele-squeeze would be advisable for the next study.

7 Summary and outlook

Flat-optics MDs were scheduled during the first and second LHC MD blocks of 2018, with 2 + 2 shifts for a total of only 32 hours. In this relatively small amount of time, the "mini-commissioning" of a brand-new machine configuration took place, demonstrating quite successfully the OP mechanics of the corresponding hypercycle (while stimulating ideas and a deeper understanding in view of possible improvements), analyzing the optics correct-ability limit together with very promising mitigation measures when operating the machine at the HL-LHC like β^* of 15 cm and telescopic index of 4 (at least in one of the two transverse planes), but also and mainly confirming the β^* reach (from the perspective of the collimation system) and the crossing angle reach of flat optics (from the perspective of the long-range beam-beam effects). Flat optics are however certainly not mature enough to restart the machine after LS2, but additional experience gained in MD during the first year of Run 3 will very likely confirm their reliability and great potential for the future operation of the LHC and HL-LHC.

Acknowledgements

The authors are grateful to G. Arduini, M. Giovannozzi, E. Métral and Y. Papaphilippou for their accurate and patient work of proofreading and commenting the draft version of this manuscript. S. Redaelli is also acknowledged for the valuable feedback he gave to the collimation-related part of the MD programme.

References

[1] S. Fartoukh, "Flat telescopic optics", ABP-HSS Section meetings 8/11/2017, https://indico.cern.ch/event/672393/.

[2] J.M. Coello De Portugal et al., "MD2148: Flat optics", *LHC MD Note CERN-ACC-NOTE-2018-0051*, 2018.

[3] S. Fartoukh, N. Karastathis, M. Solfaroli, R. Tomas, "About flat telescopic optics for the future operation of the LHC", *CERN-ACC-2018-0018*, CERN, Geneva, Switzerland, 2018.

[4] S. Fartoukh, A. Valishev, and D. Shatilov, "An Alternative High Luminosity LHC with Flat Optics and Long-Range Beam-Beam Compensation", *TUPTY073 in Proceedings of the 5th International Particle Accelerator Conference 2015*, May 3-8 2015, Richmond, VA, USA, 2015.

[5] S. Fartoukh, "Achromatic Telescopic Squeezing scheme and its Application to the LHC and its Luminosity Upgrade", *Phys. Rev. ST Accel. Beams , Vol. 16, 111002*, 2013.

[6] S. Fartoukh, "Optics repository for the 2018 flat ATS MDs", /afs/cern.ch/eng/lhc/optics/runII/2018/MDflatoptics2018.

[7] T. Persson *et al.*, "Outcome of linear optics commissioning in 2017", presented at the LHC Machine Committee no. 312, 19/07/2017. https://indico.cern.ch/event/654265/

[8] E. Maclean *et al.*, "Outcome of non-linear optics commissioning in 2017", presented at the LHC Machine Committee no. 312, 19/07/2017. https://indico.cern.ch/event/654265/

[9] E. Maclean *et al.*, "Detailed review of the LHC optics commissioning for the nonlinear era", *CERN-ACC-2019-0029*, CERN, Geneva, Switzerland, 2019.

[10] LHC elogbook, Tuesday 12$^{\text{th}}$ June 2018, morning shift: https://ab-dep-op-elogbook.web.cern.ch/ab-dep-op-elogbook/elogbook/secure/eLogbook.php?lgbk=60&date=20180612&shift=1.

[11] LHC elogbook, Tuesday 12$^{\text{th}}$ June 2018, afternoon shift: https://ab-dep-op-elogbook.web.cern.ch/ab-dep-op-elogbook/elogbook/secure/eLogbook.php?lgbk=60&date=20180612&shift=2.

[12] LHC elogbook, Sunday 17th June 2018, morning shift: https://ab-dep-op-elogbook.web.cern.ch/ab-dep-op-elogbook/elogbook/secure/eLogbook.php?lgbk=60&date=20180617&shift=1.

[13] LHC elogbook, Sunday 17th June 2018, afternoon shift: https://ab-dep-op-elogbook.web.cern.ch/ab-dep-op-elogbook/elogbook/secure/eLogbook.php?lgbk=60&date=20180617&shift=2.

[14] Monday 23rd July 2018, morning shift: https://ab-dep-op-elogbook.web.cern.ch/ab-dep-op-elogbook/elogbook/secure/eLogbook.php?lgbk=60&date=20180723&shift=1

[15] Saturday 28th July 2018, night shift: https://ab-dep-op-elogbook.web.cern.ch/ab-dep-op-elogbook/elogbook/secure/eLogbook.php?lgbk=60&date=20180728&shift=3

[16] L. Malina and J. M. Coello de Portugal, "Optics Measurements in Storage Rings Based on Simultaneous 3-Dimensional Beam Excitation", *THPAF046 in Proceedings of the 9th International Particle Accelerator Conference 2018*, Apr.-May 2018, Vancouver, Canada, 2018.

[17] S. Fartoukh *et al.*, "LHC MD2148 – Telescopic Flat Optics with Pilots and 3 10^{11}", MPP procedures, CERN, Geneva, Switzerland (2018).

[18] R. Bruce *et al.*, "Updated parameters for HL-LHC aperture calculations for proton beams", CERN-ACC-2017-0051, CERN, Geneva, Switzerland (2017).

[19] T. Persson *et al.*,"Optics and Corrections", *Proc., 10th Evian Workshop on LHC beam operation*, Evian Les Bains, France, 30 Jan – 1 Feb. 2019, CERN, Geneva, Switzerland, 2019.